Coupling of optical fibers for the Aachen Muon Detector

von

Daniel Keßler

Bachelorarbeit in Physik

vorgelegt der Fakultät für Mathematik, Informatik und Naturwissenschaften
der
Rheinisch-Westfälischen-Technischen Hochschule Aachen

Vorgelegt im Juli 2016

Erstgutachter

Prof. Dr. Thomas Bretz
3. Phys. Institut A
RWTH Aachen

Zweitgutachter

Prof. Dr. Thomas Hebbeker
3. Phys. Institut A
RWTH Aachen

Abstract

In the scope of this thesis investigations on a possible improvement regarding the practical use of optical fibers for light conduction in the Aachen Muon Detector (AMD) are performed.
Muons from cosmic ray induced air showers are detected by the scintillator tiles of AMD whose light is conducted via optical fibers onto photo sensors (silicon photomultipliers). To reliably detect muons it is crucial that as many photons as possible reach the SiPMs. In this thesis two potential photon loss factors in the light conduction system to the SiPMs are investigated. The optical transition between two fibers and the reflection at one fiber end.
To show this, at first the light conduction system is explained and it will be discussed why there is a transition between two different optical fibers. Then measurements will be shown regarding the influence of optical gel at the transition. In the second part the author verified that making one end of an optical fiber reflective, while light is induced from the lateral area, increases the light output at the non-reflecting end. For this reason several materials are tested as reflectors.
Finally this thesis will be concluded by a short summary and a discussion of the influence of these findings to the future of AMD.

Contents

CHAPTER 1

Introduction

1.1 Cosmic rays and extensive air showers

In 1912, austrian physicist Viktor Hess published an article in which he described various balloon flights to investigate the ionization of air as a function of altitude. Finding a higher ionization rate in higher altitude he concluded the existance of the so-called 'Höhenstrahlung'(-high altitude radation), later to be called 'cosmic rays' [1]. Others such as Regener, Pfotzer, Rossi, Bothe, Kohlhöster undertook further experiments and analyzed the propagation and correlation of these ionization events. Thanks to them and especially Pierre Auger it is known today, that in the atmosphere primary cosmic particles (in scope of this thesis only ionized nuclei) induce avalanche processes in which secondary particles are created. These avalanches are called extensive air showers. Auger was the first to calculate back the energy of the primary particle by measuring the secondaries reaching ground and estimated an energy of around 10^{15}eV. [2] [3]
Because of these extremely high energies, a lot of new particles were discovered by understanding the extensive air showers. For many years the question of the sources of these high energetic particles, and what accelerates them, remained. For the highest energies it is still not known. [2]

1.1.1 Cosmic rays

After several decades of cosmic ray measurements, cosmic rays with energies between 10^6eV and 10^{20}eV were found. Whereas the flux of particles with higher energies is significantly lower than the one of those with lower energies.
In figure 1.1 it can be seen how the flux is depending on the energy where there are four main regions. Each region can be described as a power function $F(E) \propto E^{-\gamma}$ with a different spectral index. The flux 'F' is usually given in units of one over area, solid angle and time.
The first region is up to the *cosmic ray knee* at $\approx 10^{15}$ eV with a spectral index of $\gamma = 2.7$.

Then there is the region up to the *cosmic ray ankle* at $\approx 3 \cdot 10^{18}\,\mathrm{eV}$ ($\gamma = 3$) and the one up to the *cut-off* at $\approx 3 \cdot 10^{19}\,\mathrm{eV}$ ($\gamma < 3$). For even higher energies the flux decreases significantly, but it is unclear how exactly. [2] [4]
Those particles with energies above $\approx 10^{18}\,\mathrm{eV}$ are called 'Ultrahigh energy cosmic rays' (UHECR)[2].

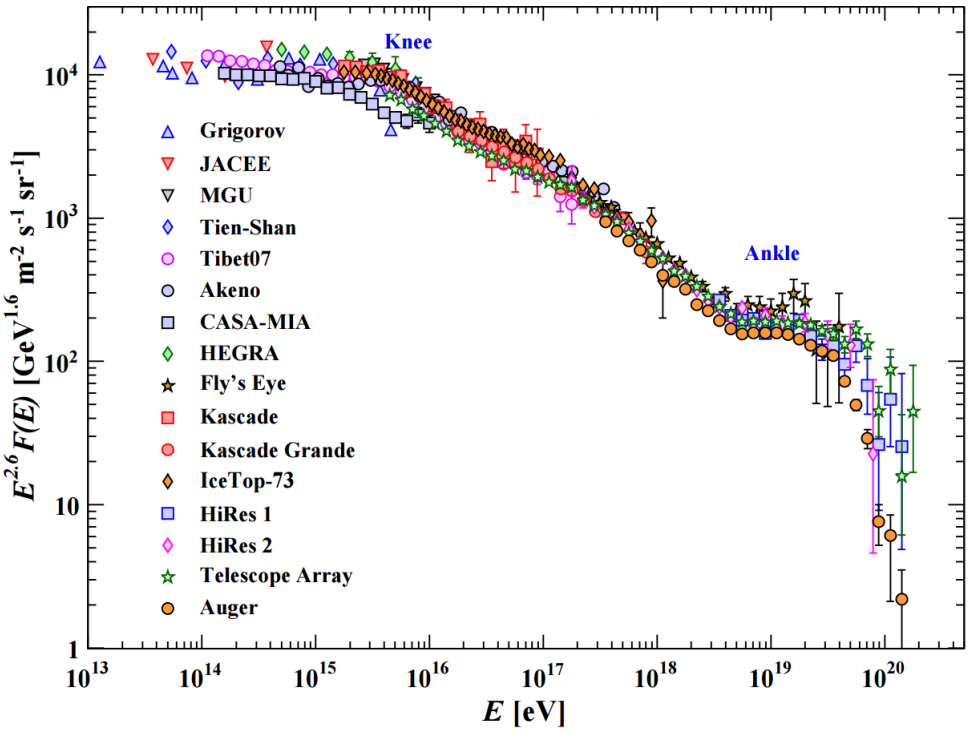

Figure 1.1: The cosmic ray spectrum at the highest energies, scaled by $E^{2.6}$ to emphesize features like the knee and the ankle. The plot combines the results of several experiments until 2015. Adapted from [4].

There are assumptions of different origins for cosmic rays with different energies. The very common idea is, that up to the ankle, the most particles are of a galactic origin, like shock fronts of supernova remnants. They would be 'captured' in the magnetic field and be accelerated again and again until their energy is high enough to escape. This would explain the knee. Because the maximum energy depends on the charge of the particle, heavier particles can be accelerated higher. At the knee the maximum energy for a single proton is reached. Up to the ankle more and more heavier particles like He, O and Si cannot accelerated any further.
Then at the ankle the flux is dominated by cosmic rays from outside the milky way, hence, by a extragalalactic flux. These particles could have origins like active galaxies or jets of black holes.
At the cut-off any proton, whose origin is farther away than $\approx 200\,\mathrm{Mpc}$, should theoretically lose energy by interactions with photons of the cosmic microwave background, initiating the so-called 'GZK-cutoff'. So one should not be able to detect particles with higher energies.
The fact, that several particles have been measured with energies above $10^{20}\,\mathrm{eV}$ is one

reason why there is so much work put in the investigation of UHECR. Theoretically they cannot have an extragalactical origin, but on the other hand there are no certainly known mechanisms in our galaxy that would explain them. [2] [4]

1.1.2 Extensive air showers

Because of the extreme difficulties to get big enough detectors very high in the atmosphere to directly measure the high energy cosmic rays, most detectors measure them indirectly through extensive air showers at ground. For example, a primary particle with around 10^{19}eV produces more then 10^{10} particles at sea level. In scope of this thesis with 'cosmic rays' only charged nuclei are meant. The produced particles result from an interaction of the hadronic primary particle (cosmic ray) and a nucleus in the atmosphere (see figure 1.2). In this interaction mesons are created, which then decay in an electromagnetic, a muonic, and a hadronic component.

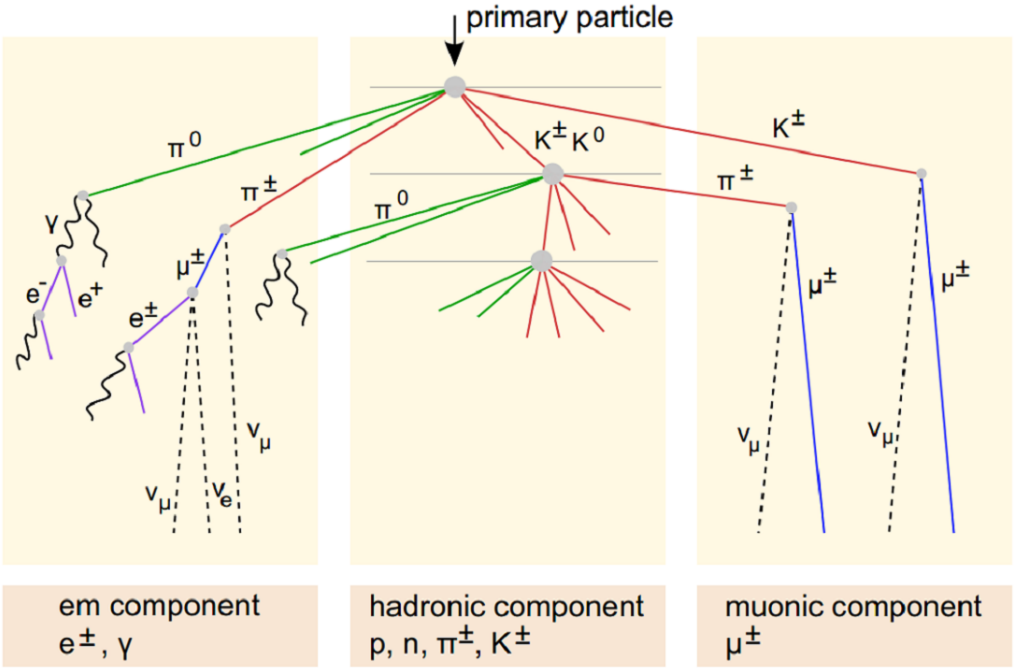

Figure 1.2: Scheme of extensive air shower development. A primary particle creating light hadrons and mesons, of which the electromagnetic (em), muonic and hadronic components evolve. Taken from [5].

The most produced particles are of the em-component. Hence, about 85% of the energy is deposited in electrons and positrons, while around 10% is transported via muons and only some 4% is located in the hadronic component. [2]

An extensive air shower has several properties, from which one can deduce the arrival direction of the primary particle as well as its mass and energy.

Highly dependent on mass is the depth of maximum particle production in the atmosphere X_{max}. The heavier the primary particle, the higher the altitude of the maximum particle production. According to Heitler, for the em-component applies:

$$X_{max} \propto ln(E_{primary}) \tag{1.1}$$

Regarding the muonic component, from the generalized Heitler model of hadronic air showers results that the number of produced muons is almost linear with the energy of the primary particle and proportional to a small power of its mass [6]:

$$N_\mu = \left(\frac{E/A}{\zeta_0}\right)^\beta \cdot A \tag{1.2}$$

with A being the mass of the primary, ζ_0 being the critical energy at which charged pions decay into muons and $\beta \approx 0.9$. [6]

1.2 Pierre Auger Observatory

Due to the fact, that the quantity of UHECRs depends on area and time, the only way to measure more events is to build larger detectors.
The Pierre Auger Observatory is the largest experiment of its kind in history. In Argentinia, in the province of Mendoza, it covers an area of around $3000\,\mathrm{km}^2$. It is taking data since 2004.
The observatory operates with a hybrid detector design (figure 1.3). There are four fluorescence detectors (FD), which measure the fluorescence light of air showers, so the development of the air shower in the atmosphere; and 1660 ground-based surface detectors (SD), which are basically water tanks to measure the Cherenkov light produced when charged particles propagate with velocities higher than the speed of light in water, so measuring the lateral distribution of the secondaries on the ground.

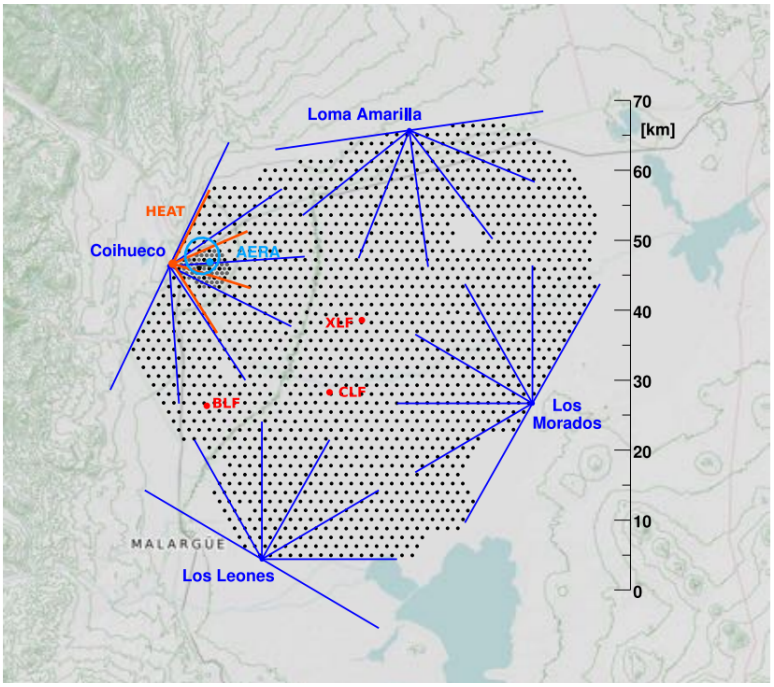

Figure 1.3: Layout of the Pierre Auger Observatory. The dots represent the surface detector stations (SD). The four fluorescence detector sites with their fields of view (colored lines) are shown. Taken from [7].

The big advantage of this hybrid design is that one air shower is measured by two different detector systems. While each measurement alone may have large systematic uncertainties, the combination of both can reduce them. [8]
Especially through observation of the air shower path via the fluorescence light detectors, a better energy resolution is possible, than with surface detector stations only.

1.3 The Aachen Muon Detector

Deducing the mass composition of cosmic rays from measurements of air showers is attended by large uncertainties due to the hadronic component, whose interaction properties are not yet fully understood. Hence, these uncertainties can be reduced by measuring different mass-sensitive observables [6]. At the Pierre Auger Observatory, at the moment the most mass-sensitive observable is X_{max}. This can be determined by the fluorescence detectors.
Another mass-sensitive observable is the muon number. With the current surface detectors, the Cherenkov water tanks, only statistical information about the muonic component can be deduced. So, to directly measure the muon number, an additional detector is needed. As part of the AugerPrime-upgrade such a detector system is planned to be installed [7]. At the RWTH Aachen a prototype of such a detector has been developed and built: The Aachen Muon Detector.

This detector is supposed to be installed beneath the existing surface detector sta-

tions. For this purpose it is built with a solid waterproof steel case. By laying it beneath the water tanks, which serve as shielding for electrons, a higher fraction of the incoming particles are muons.

For reasons of a better handling, each detector consists of two identical halves (see figure 1.4). Each half is built in a modular design with four trays, of which each holds eight scintillator tiles, and a fifth tray which contains electronics. At the end of each tray sits an SiPM carrier board to measure the scintillator light. The SiPMs and the tiles are connected via optical fibers. [5] [9]

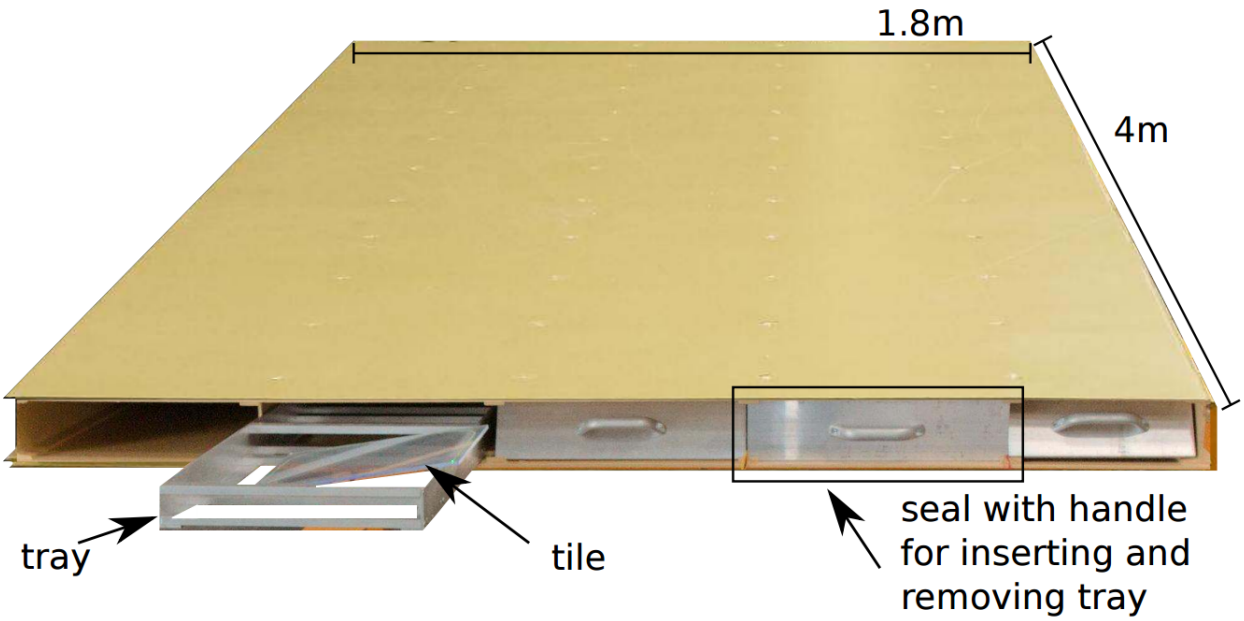

Figure 1.4: Photography of one identical half of the Aachen Muon Detector. The case is made of steel, so it is solid enough to be installed under the SD water tanks. Each of the four bigger trays contains eight scintillator tiles, so that the whole detector consists of 64 tiles. The tray on the very right holds electronics. Taken from [5].

CHAPTER 2

Light collection and conduction inside AMD

The light conducting system consists of a wavelength-shifting fiber which is glued in each scintillator tile in purpose to collect the light the scintillator tiles produce by particle fly-throughs. Due to its non-optimal conduction properties there is a transition to a transparent optical fiber, which conducts the light to the SiPMs.
In this chapter each part and its theoretical functionality is described shortly in regard this this thesis.

2.1 Scintillator tile

For AMD, the EJ-212 plastic scintillator from Eljen Technology [10] is used. Plastic scinitllators are organic scintillators, which work like the following:
The energy of an incoming particle is absorbed by the molecular structure of the scintillator material. This excites the molecules into a higher energy level. By de-exciting over non-radiative and radiative energy level transitions fluorescence light is emitted.
The chosen Eljen Technology scintillator emits this fluorescence light with a wavelength of the blue color spectrum.

In order to reduce losses of the fluorescence light, the first prototype tiles are wrapped in diffusely reflective materials like Tyvek or PTFE. As the handling of Tyvek is better and the light yield is similar, all the other tiles are going to be wrapped only with Tyvek. This reflects the light back into the tiles.

2.2 Wavelength-shifting fiber

To collect the fluorescence light inside the scintillator and to guide it to the photosensor, a wavelength-shifting fiber (WLS) is used. At AMD the type BCF-92 from Saint-Gobain

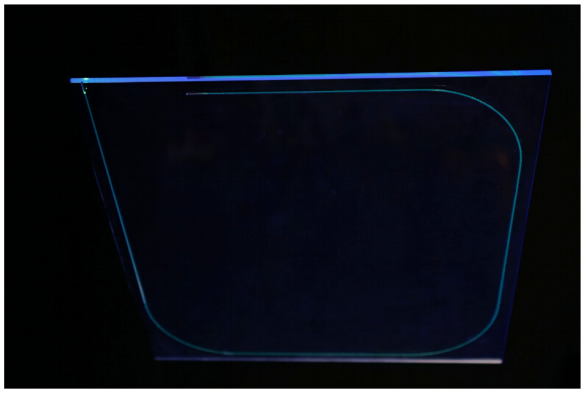

Figure 2.1: Picture of a unwrapped tile. Adapted from [5].

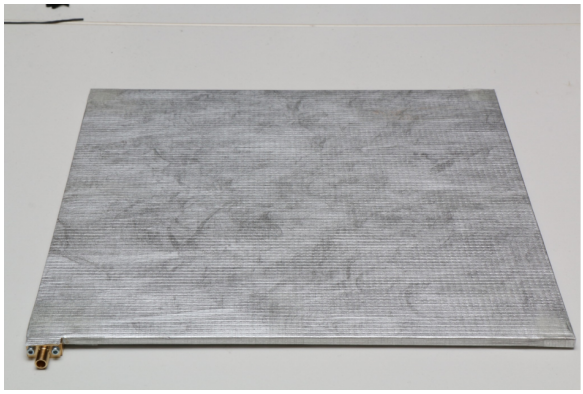

Figure 2.2: Tile wrapped in Tyvek. Taken from [5].

is used [11]. The fiber is glued in the scintillator in a sigma shape (figure 2.1) so that one end is inside the tile and the other ends some millimeters outside. There, it is coupled to a transparent optical fiber.
For the first prototype tiles the end inside the scintillator has been painted with a chrome paint spray to make it reflective, so that at best all the light is conducted to the outer end.
WLS material works similar to the principle of the scintillator material. Incoming photons excite the molecules of the WLS, which then de-excite over several energy level transitions and conversions. In the end, the absorbed blue light is shifted to green light (figure 2.3).

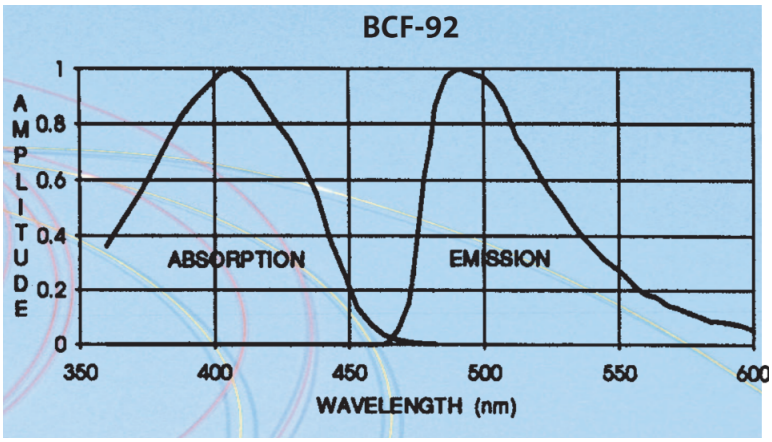

Figure 2.3: Spectra of absorption and emission of the WLS fiber. The maximum of the absorption spectrum is at a blue wavelength, whereas the maximum of emission is at a green wavelength of 500nm. Taken from [11].

The fiber collects the light in the following way: A photon with a wavelength appropriate to blue light enters the WLS fiber, there it gets shifted to green, but not necessarily in the same direction because the emission is isotropic. The light rays propagating at an angle larger than the critical angle α_{crit} for total internal reflection are trapped in the

fiber (figure 2.4). [12]

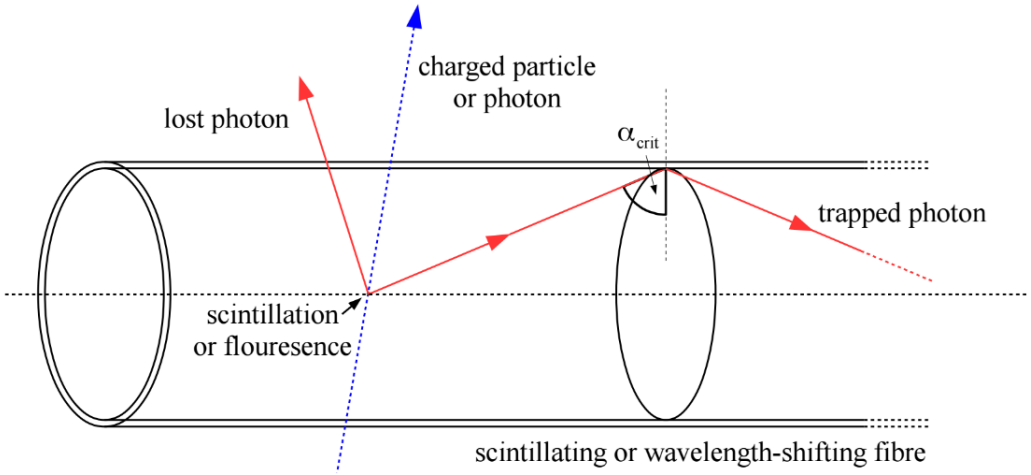

Figure 2.4: Schematic of light trapping in a WLS fiber. A primary photon is absorbed in the WLS material and is wavelength-shifted. The shifted photons are emitted isotropically so that the ones with an incidence angle at the core-cladding interface larger than the critical angle α_{crit} for total internal reflection are trapped. Taken from [12].

This WLS fiber has an absorption length or attenuation length of around 3.5 m. It describes how long the light can propagate through the fiber until its intensity is reduced to $1/e$. This loss results of photon absorption in the fiber material.

2.3 Optical fiber and transition

Due to its rather short absorption length the WLS fiber is not practical to conduct the light all the way to the SiPMs, which is up to approximately three meters. Instead shortly after exiting the tiles the WLS fiber is coupled to a transparent optical fiber.
This fiber (the ESKA CK-40) has a much longer absorption length [13].

For the coupling a special clamp is used in which the both fibers are lead together and being fixed in position.

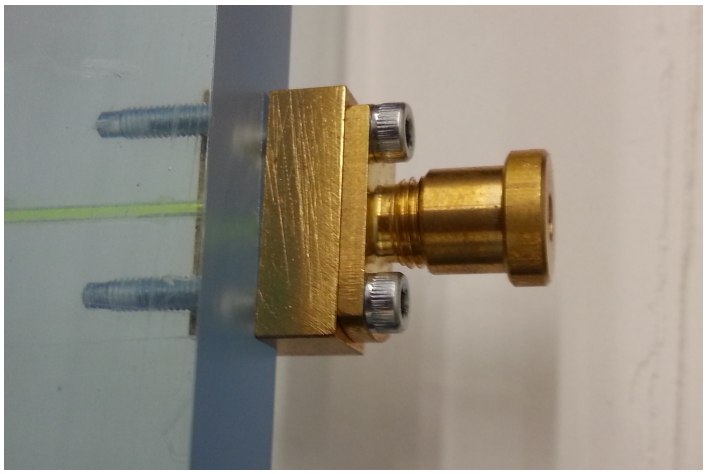

Figure 2.5: Clamp to couple the WLS fiber to the transparent optical fiber attached to a test tile.

Figure 2.6: Unscrewed disassembled clamp.

The important information about the fibers are summarized in the following table:

fiber	refractive index (core)	acceptance angle
transparent fiber	1.49	61°
WLS fiber	1.60	35.7°

2.4 Coupling to SiPM

From each tile an optical fiber leads onto one SiPM, hence in AMD 64 SiPMs are installed. The SiPMs of type S12571-050P from Hamamatsu [14] are being used. SiPMs are stable semiconducting photo detectors with high photon detection efficiency and low operating voltages, which are one key component of AMD.
The fibers are coupled to the SiPMs with special clamps, that allow a precise adjustment onto the SiPM. At the current state, there is still a small gap of air between the fiber and the SiPM. Hence, with a additional optical coupling, instead of an only mechanical one, there might be some improvements possible. However, to guarantee maximal flexibility of the prototype, it is not yet glued or stuck onto the SiPMs.

2.5 Investigations on possible light losses

At the time of this thesis there were discrepancies between the measurements of the first prototype tiles and the simulation of this system. Simulations show four to five times more light coming to the SiPMs than what was seen in first measurements (see appendix, section 6).

In hope of finding the reason for those differences the author investigates on two different possibilities of light loss in scope of this bachelor thesis.
First by measuring the possible advantages of optical gel at the coupling of the wavelength-shifting and optical fiber (chapter 3). And the other is the reflection at the wavelength-shifting fiber end inside the scintillator tile (chapter 4).

CHAPTER 3

Fiber coupling

In order to find possible losses of intensity, the first property, which is investigated in this thesis, is the coupling of a WLS fiber to a transparent optical fiber.
In this chapter, at first a theoretical description of the coupling follows. Then the basic idea of the experiment and of its setup is given. After that, measurements are shown and systematics are discussed. In the end, the results are summarized and consequences are concluded.

3.1 Theory

Reflection and transition of electromagnetic waves, e.g. light, at an interface is theoretically described by the Fresnel equations. Calculations of how much light is reflected and how much gets through the transition area in dependence of angle, polarization and refractive indices are possible.
Under the assumption, that half of the light is p-polarized and the other half is s-polarized and that the materials are perfectly dielectric and non-magnetic, the following formula is being used to calculate the reflectance at each transition [15]:

$$R = 0.5 \cdot \left(\frac{tan(\alpha - \beta)}{tan(\alpha + \beta)} \right)^2 + 0.5 \cdot \left(\frac{sin(\alpha - \beta)}{sin(\alpha + \beta)} \right)^2 \tag{3.1}$$

Whereby α is the angle of incidence. β is the angle of refraction and can be calculated by the Snell's law $\left(\frac{n_1}{n_2} = \frac{sin\beta}{sin\alpha} \right)$.

In figure 3.1 the angular distribution of light inside the WLS fiber is calculated back from a measurement of the angular distribution of light exiting the fiber into air. This measurement was performed by Simon Nieswand [12].

Here most of the light inside the fiber propagates at an angle of about 20°. So, one can calculate the reflectance for each transition. In the ideal case this is the direct transition

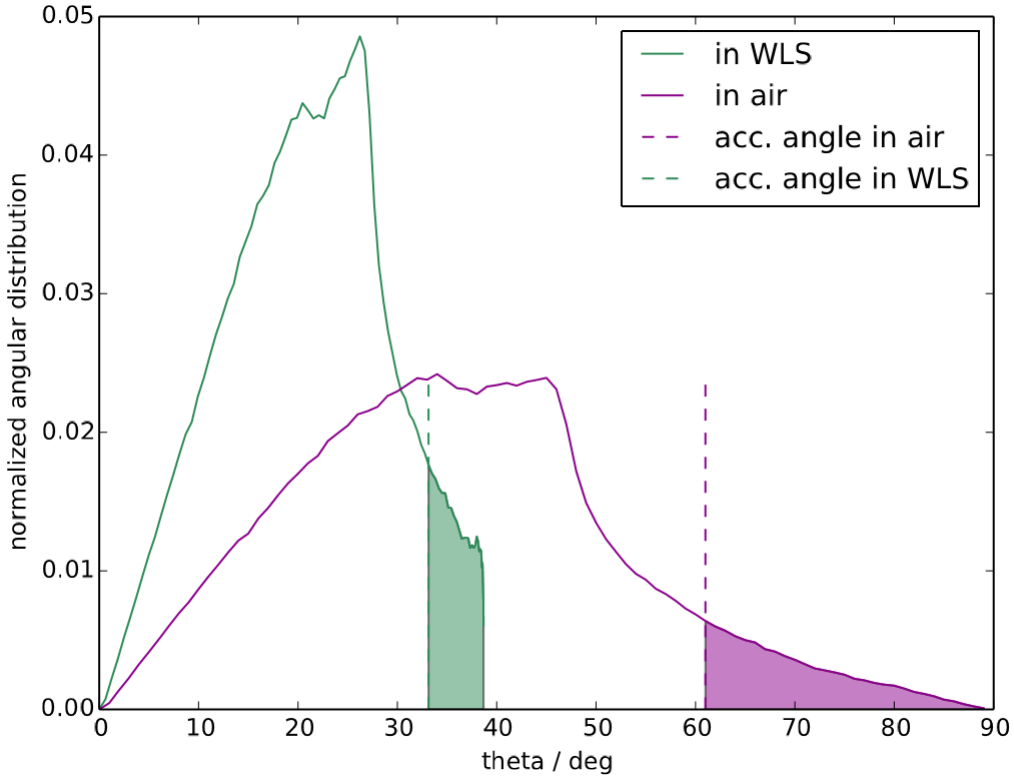

Figure 3.1: Angular distribution of light exiting a WLS fiber into air (violet) [12] and from that calculated back, the angular distribution of the light inside the WLS. The shaded areas mark the amount of light that is not induced in the transparent fiber due to the acceptance angle of 61%. This loss of approximately 8% cannot be avoided.

from the WLS fiber to the transparent optical fiber. However, due to the design of the clamp, one cannot verify the direct coupling and due to possible imperfections at the fiber ends, there could be an air rim and hence a bigger loss of light.

Transition (refractive index)	Reflectance (R)
WLS (1.60) ⇒ air (1.00)	0.056
air (1.00) ⇒ opt. fiber (1.49)	0.041
WLS (1.60) ⇒ opt. fiber (1.49)	0.001

The transition for three layers is given by:

$$T = \frac{T_{12} \cdot T_{23}}{1 - R_{12}R_{23}}$$
$$\Leftrightarrow T = 1 - (R_{12} + R_{23}) + \mathcal{O}(R^2)$$

Whereby T is the transmission coefficient and the relation $T = 1 - R$ was used. The indices stand for the interface to which the particular coefficient refers. E.g. R_{12} is the

reflectance for the transition from the first to the second layer.

Hence, the loss due to reflection when air is between the fibers (layer 1: WLS, layer 2: air, layer 3: opt. fiber) is about 9.7% based on these calculations. Whereas when the coupling is ideal and there is no air between the fibers, the loss would only be about 0.1% !

A possible solution to avoid air between the fibers would be the use of optical gel with a refractive index almost identical to that of the fibers.
If the fibers would not be clamped directly end to end, the gel should theoretically displace the air, and hence there would only remain the transition from WLS fiber to gel and the one from gel to optical fiber. The optical gel *BC-630* from Saint-Gobain with an refractive index of 1.46 [16] is investigated. The reflection loss for the complete transition (WLS to gel and gel to opt. fiber) results in about 0.2%, what is a negligible amount of light.

Nonetheless at best the fibers are directly connected to each other without any air in between.

3.2 Experimental setup

A practical way to find out if gel in between the fibers would increase intensity, is to compare the light output after the coupling one time without gel and one time with gel in a well accessible and changeable experiment.
With the following setup, built with Thorlabs equipment, exactly this is possible.
It is important to note that only relative measurements in comparison to each other are possible. No absolute intensities in regard to AMD are determined.

For the experiment a perspex test-tile with a WLS fiber glued inside is used. The fiber overlaps the tile on both sides. At the end with the clamp it sticks out approximately 0.3 cm , while on the other side about 5.7 cm. At the tile the clamp for the fiber coupling is screwed. The tile is fixed on a Thorlabs platform. Then there is a holding for the transparent optical fiber. The WLS fiber end on the other side of the tile is stuck in a Ulbricht-sphere from Thorlabs itself. A Ulbricht-sphere uses diffuse reflection to homogenize incoming light. It is needed as in one hole of the sphere a LED is screwed. The light shall be homogeneous, so that a detector can be connected to the sphere, as well as the amount of light entering the fiber should be stable. This way the intensity of the LED can be monitored while light is induced into the fiber.
By installing another detector at the end of the transparent optical fiber, the intensity that goes through the coupling can be measured relatively to the (not absolute) intensity of the LED. This way effects of changes in the coupling can be compared.

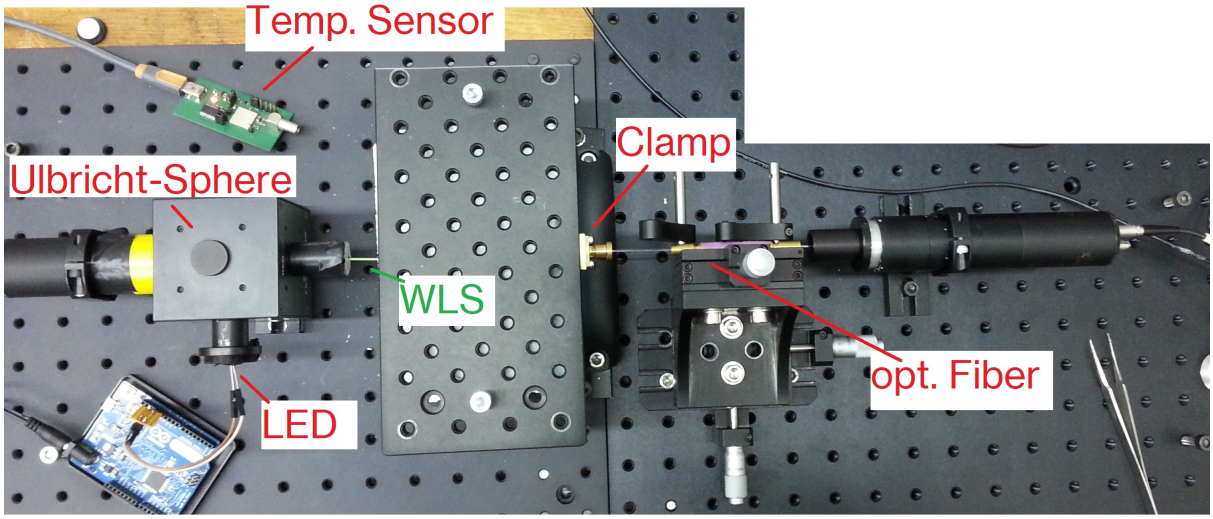

Figure 3.2: Experimental setup to measure changes in the coupling of the WLS fiber and the optical fiber. Light is produced by a LED in a Ulbricht-sphere, so that a control measurement can be taken. It is then lead through the WLS fiber and the optical fiber into a second detector.

The following elements are used:

- Detectors: pin diodes
- Each pin diode is read out by a picoammeter: the 6485 Picoammeter from Keithley. A picoammeter measures very low electric current, like the ones occurring in the pin diodes.
- LED: (UV+blue)-LED. The wavelength mixture of the LED is similar to the scintillation light that would be produced by the scintillator tiles.

The picoammter are controlled and read out by a PC via USB. The original program, of the used one, is with little changes taken from the AMD work group of the institute.

3.3 Validation of experimental setup

All measurements were taken in a laboratory with darkened windows. During the experiments the light was switched off so that only a very small amount of ambient light could possibly reach the setup.

In very first measurements, it it has been investigated, that the LED needs about ten minutes to warm up and produce constant light, as well that the detectors need about twenty five minutes to measure constantly.
After the warm up time, the random noise is only a very few per mill.
It is important to note, that the detectors need to run to warm up. Just plugging the picoammeter into the computer does not start the warm up process of the detectors.

To ensure reasonable comparisons, a offset-test was made. Without changing anything, several measurements were taken with a few minutes apart. During the pauses the detector did not measure, but apparently did not cool down much as well. Its deviation is only a few per mill, too. That is much less, than the to be examined effects. So it can be neglected. The same test was made with a few hours and a new warm up phase between the measurements. The difference was still in the same dimension.

3.3.1 Temperature

Due to the fact, that the detectors and the LED need some time to warm up, the measurements are apparently temperature dependent. Hence a change of temperature in the laboratory would influence the measurements.

To find out what the deviation through temperature is, a temperature sensor [17] read out by a Hamamatsu chip was also connected to the computer. Temperatures were taken on several days and several times of day.

The work room is air-conditioned, so that no bigger differences were expected. The maximal difference of temperature is about $1.1°C$, whereas the difference in intensity is about three per mill. It cannot be excluded that this is just the deviation of the offset.

Even though the temperature should change rapidly, it should not distort the measurements significantly. Nevertheless rapid changes in temperature are very unlikely due to the air conditioner.

3.4 Investigations on an optimized setup

3.4.1 Procedure

After the basic requirements for a comparison are met, a first comparison measurement can be taken.
For that purpose a series of measurements without gel in between the fibers were taken. When inserting the fiber into the clamp, it has to be paid attention that the fiber is not stuck on any small resistance in the clamp. Sometimes it gets a little stuck, even though one can push it in some more millimeters.
Then a series of measurements with gel in between, where the gel was positioned in the disassembled, but fixed, clamp (unscrewed upper half - see figure 3.3). After that, a series of measurements with gel positioned from the top of the clamp (figure 3.4) were taken.

To fill gel into a disassembled clamp seemed easier to handle.

For one series of measurements two times three measurements of 250 data points were taken. During each three measurements nothing was changed. Between the two times, the fiber was pulled out of the clamp and stuck back in it again. After that, the fiber

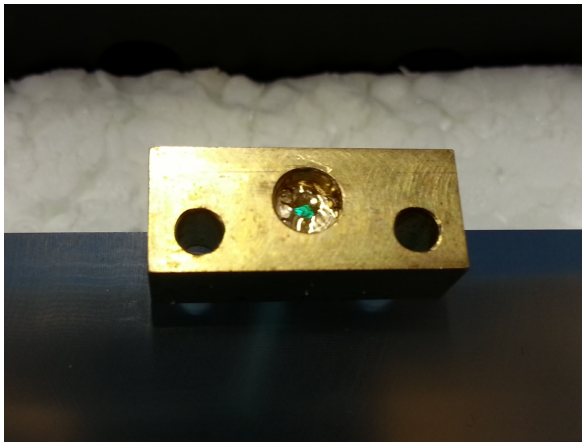

Figure 3.3: Gel filled in the disassembled clamp.

Figure 3.4: Gel filled from the top of the clamp.

was pulled out and stuck back in for three more times, but with only one measurement of 250 data points in between. Gel was only filled in one time each series and not every time the fiber was stuck back in.

3.4.2 Comparison of coupling with and without gel

In figure 3.5 the measurements without gel are shown.

The same series of measurements were taken with the two methods of filling gel in, too (figure 3.6 and 3.7. In the second, a significant uncertainty is recognizable (see section 3.4.3).

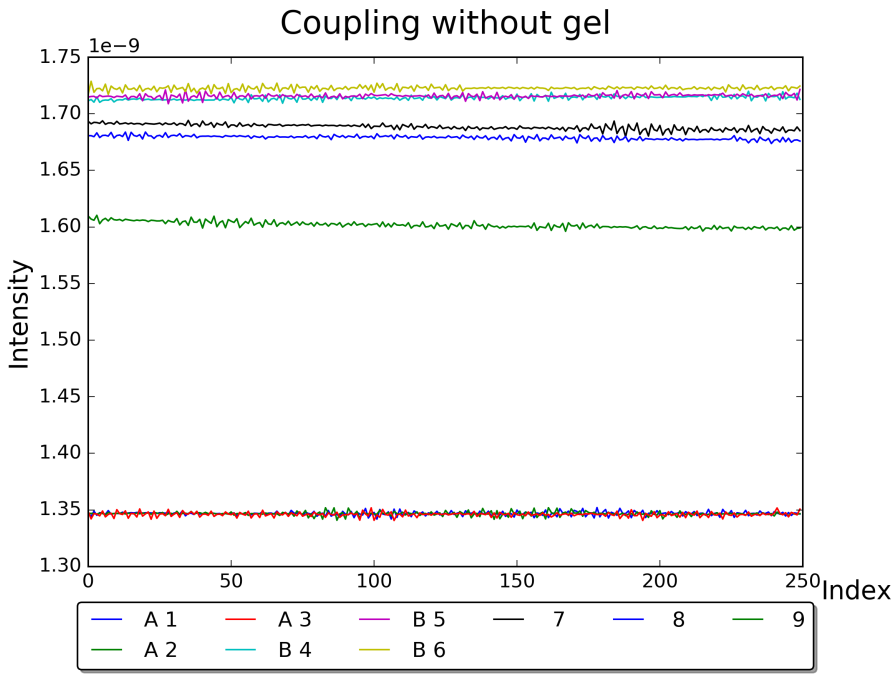

Figure 3.5: Coupling without gel in between the fibers. On the x-axis the number of each data point is shown, hence the time (≈ in seconds). In the legend the different measurements are assigned. During the first (A) and second three measurements (B) nothing has been changed. Between the two, and before each of the last three measurements, the fiber has been pulled out and stuck back in the clamp again.

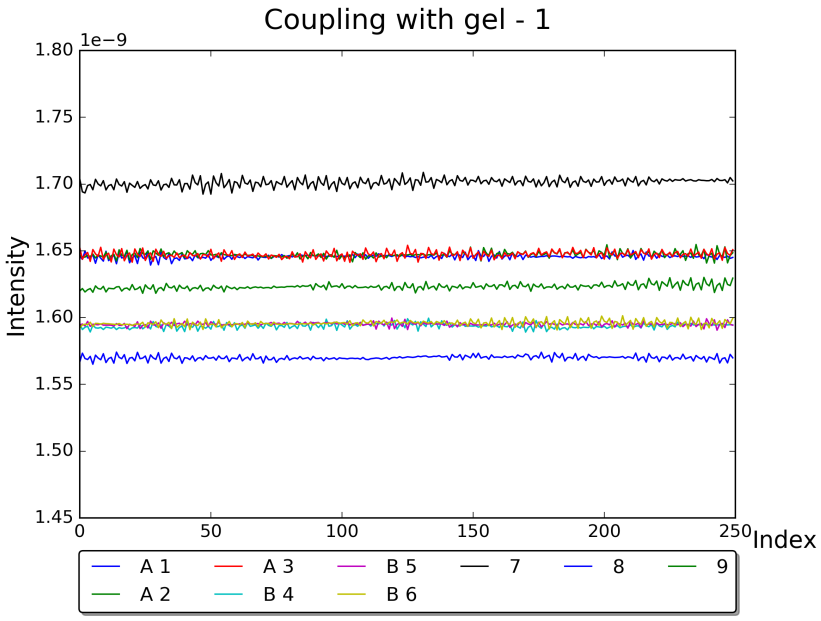

Figure 3.6: Coupling with gel filled in through a disassembled clamp. On the x-axis the number of each data point is shown, hence the time (≈ in seconds). In the legend the different measurements are assigned. During the first (A) and second three measurements (B) nothing has been changed. Between the two, and before each of the last three measurements, the fiber has been pulled out and stuck back in the clamp again. Gel was filled in only once.

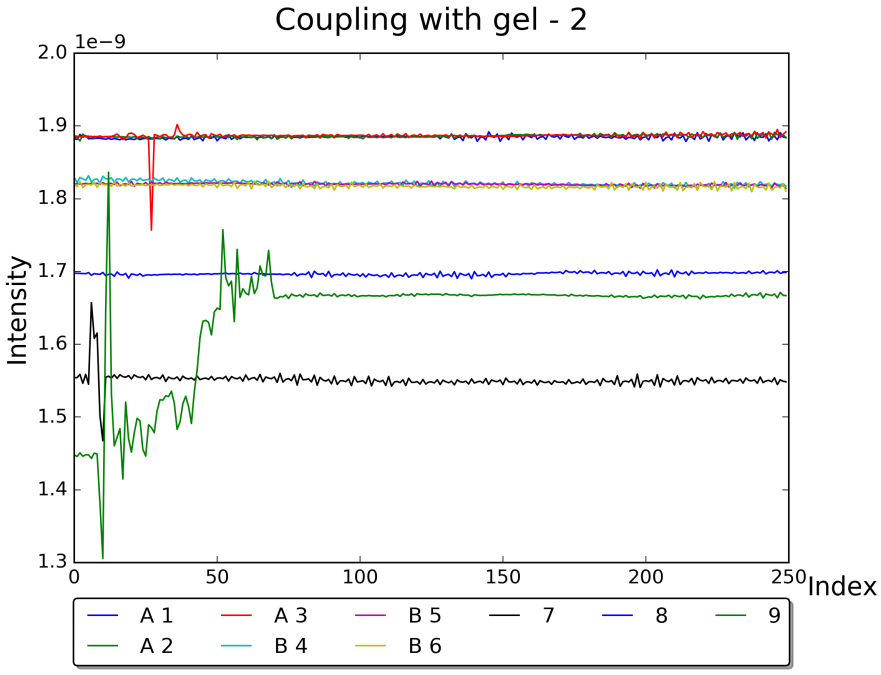

Figure 3.7: Coupling with gel filled in from the top of the clamp. Clearly recognizable: a uncertainty due to the detector position (see section 3.4.3), which here result from minimal movements of the detector and indicate uncertainties in the same dimension as the improvement relative to the no-gel coupling (green curve).

In the following table the average intensities with its estimated RMS, calculated through its variances of each time the fiber was stuck back in, as well as their mean maximal deviation are shown:

	(Intensity $\pm$ rms $\pm$ maximal deviation) $\cdot 10^{-9}$
w/out gel	$1.606 \pm 0.068 \pm 0.185$
gel1	$1.627 \pm 0.023 \pm 0.065$
gel2	$1.718 \pm 0.061 \pm 0.167$

The comparison to the measurements with gel shows, that gel may lead to a better coupling of about 7%. On the other hand, the different intensities have uncertainties in the dimension of several percents and lay within their error ranges.

During all measurements the control detector at the LED measured a constant intensity with deviations of only some per mill.

With uncertainties that high, it cannot be guaranteed that the coupling with gel is better than the one without gel. A tendency that it might be better is recognizable. Hence, the uncertainties should be reduced (see next section).

3.4.3 Consequences

Every time the optical fiber is pulled out and stuck back in the clamp, the detector has to be displaced and positioned over the fiber again. The author assumed that the big deviations between each time the fiber is stuck in again, comes from the uncertainty with which the detector can be positioned. The influence of the detector position became visible in figure 3.7, measurement 9. As a test the detector was slightly moved for approximately one millimeter and the intensity changed rapidly and severely. The fluctuation of this measurement is between $1.30 \cdot 10^{-9}$ and $1.83 \cdot 10^{-9}$ in units of intensity equivalents. Hence, the scope of the uncertainty due to the detector position is approximately as big as the scope of deviation between the measurements!
To reduce this uncertainty a guideway was built onto the Thorlabs platform, which ensures that the detector is positioned always at the same spot, as one can see in figure 3.8. In the following experiments the detector will always be positioned ten times, so that a arithmetic average can be calculated. The uncertainty of this average, hence the uncertainty through the detector position, can then be determined by calculating the variance of these ten measurements (see next section). Because the single 250 point measurements are very constant, each of the ten measurements will be just consist of twenty data points.

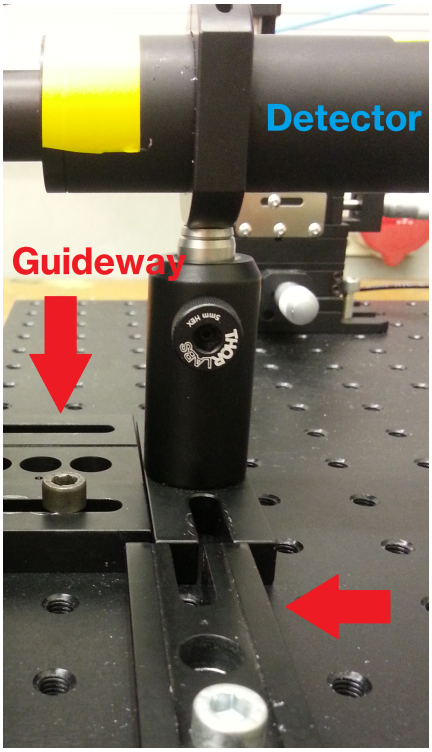

Figure 3.8: Guideway for the detector to reduce the uncertainties due to the detector positioning.

Another uncertain factor is, whether the gel is really in between the fibers and whether there really is no air left. Because the actual coupling is inside the clamp, one cannot proof that only gel is in between the fibers.
To make it checkable, the clamp has been screwed some millimeters in front of the tile.

By this way, the coupling is open and easy accessible (see figure 3.9).

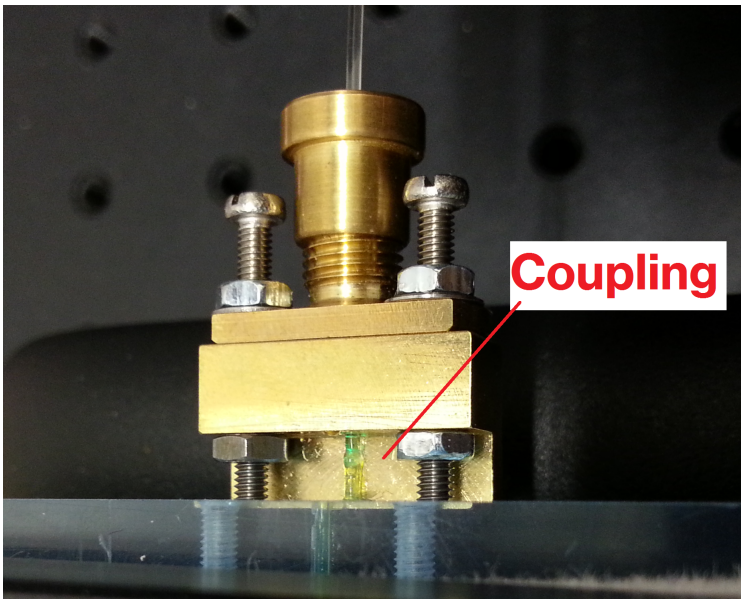

Figure 3.9: Clamp attached with a distance of some millimeters to the tile, so that the coupling is visible and accessible. Here, gel is positioned between the fibers.

Even though one cannot prevent that gel touches the lateral area of the fibers, it should not make any bigger problem, because of the multicladding of the fibers. On the one hand, the gel has a similar refractive index as the one from the fiber cores, but on the other hand, the claddings have smaller and smaller refractive indices (inside to outside), so that the light does not get lost through the lateral area.

3.5 Final comparison of coupling with and without gel

3.5.1 Procedure

For an improved measurement the results of the first measurements were taken in mind. With the clamp screwed in a distance of a few millimeters from the tile, and the guideway positioning the detector, two sources of uncertainty are reduced.
In addition, the procedure of measuring has been changed. Each time a measurement of gel is directly compared to a measurement without gel. Both measurements are taken directly after each other. For each new series of this measurement, the maximum of intensity through fiber rotation was set up. Each measurement consists of ten repositions of the detector, from which an arithmetic average is calculated. By this way, twelve measurements are taken. The one half with the transparent optical fiber, which was used in the first comparison too, and the other half with a new transparent optical fiber. The first one might have been worn out at the ends, due to the many couplings. A possible

adulteration of the experiment due to this reason should be prevented. Hence a total number of 60 single measurements of gel and 60 measurements without gel for each fiber are taken.
That means, for every series of ten measurements the fiber is stuck one time into the gel, and not, like in the first comparison, several times. Thus the chances of air getting between the fibers is even smaller.

For the comparison the difference of the intensity of gel and no-gel for every twelve measurements is calculated. Then the improvement from gel to no-gel is expressed in percentage.
The uncertainties are calculated with a quadratic error propagation of the variances of each ten measurements.
The uncertainty through the detector position a systematic effect for each single measurement. Through multiple repositions this uncertainty is estimated via calculating the sample variance. In figure 3.10 it is clearly recognizable that the intensity is not uniformly distributed. Instead, a gaussian estimation seems insofar reasonable, that adding the uncertainties quadratical has a motivation. Figure 3.10 shows the deviation of all 60 intensities for gel and no-gel for each fiber. Each bin has a poisson error, but for this regard it is not shown in the histograms.

The statistic uncertainty of each measurement of twenty data points is of the dimension of per mill, hence for the average each ten measurements in the range sub per mill. In comparison to the deviation through the detector position this is negligible small.

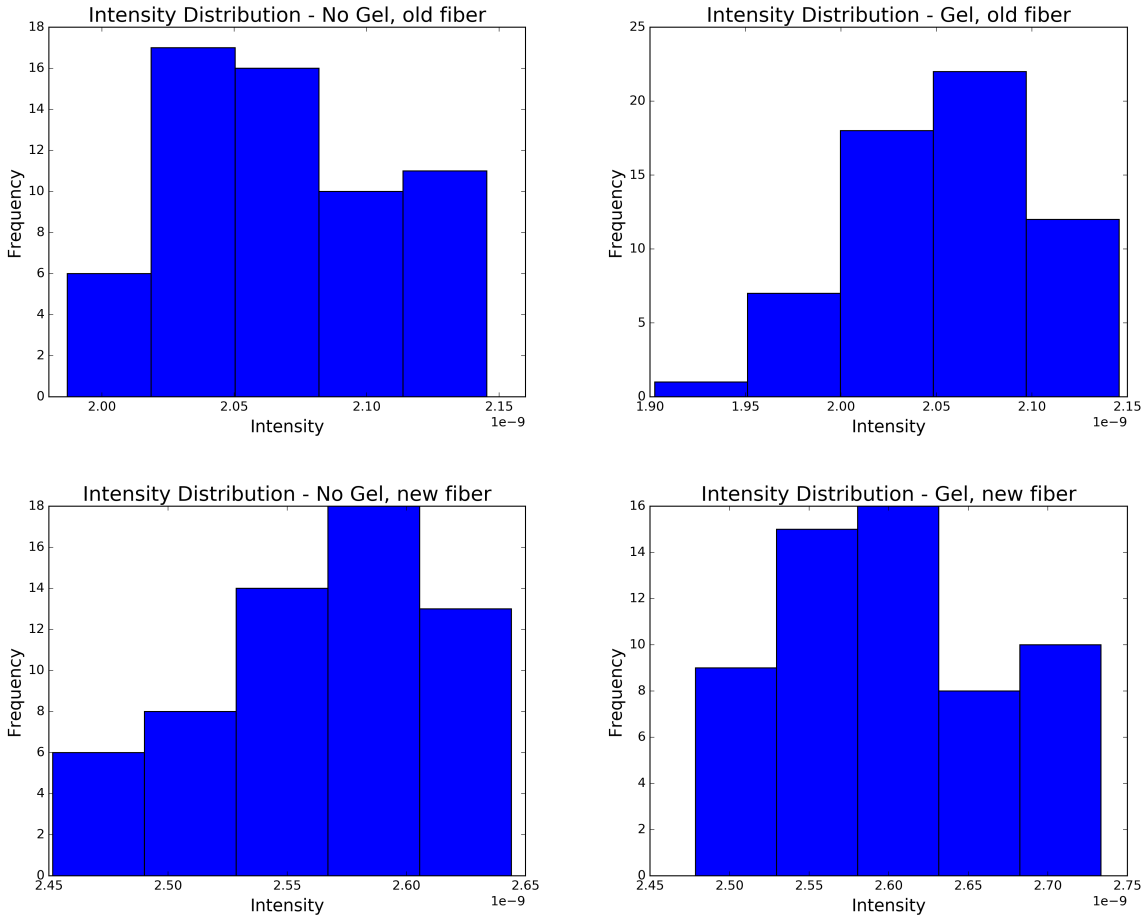

Figure 3.10: Distributions of the intensities of each fiber and coupling combination. Each histogram contains 60 measurements. A non-uniform distribution is recognizable.

3.5.2 Comparison

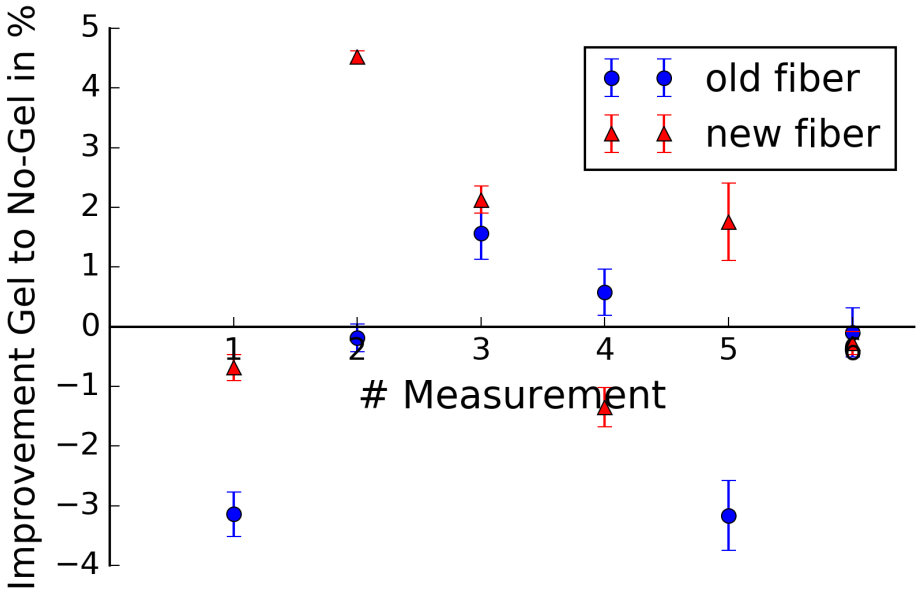

Figure 3.11: Comparison of gel coupling to no-gel coupling. The blue dots show the improvement from gel relative to no-gel with the older optical fiber. The red dots show the data of the newer optical fiber. The order is random and old and new fiber were measured independently. The deviation of the values is much larger than their error ranges. No significant trend is recognizable.

By analyzing figure 3.11 it became visible, that the different measurements are not compatible within their uncertainties. The comparison shows, that the deviation of the improvements is too big, as that it would be clear that gel is a significant improvement to no-gel coupling. The fact that the deviation of the values is much larger than their error ranges, indicates a missing uncertainty.

Such a possible uncertainty, which is not yet considered, is the deviation due to rotation of the optical fiber. When the fiber is pulled out and stuck back into the clamp one cannot be sure that the fiber is not rotated a very few degrees. This is investigated in the following section.

The detailed values of this measurement are shown in the appendix in table 6.1.

3.5.3 Uncertainty due to fiber rotation

To estimate the uncertainty due to fiber rotation, multiple measurements were performed. At first the fiber (in the setup from above) was rotated to find the maximum and ten

series of data points were taken. Then the fiber was pulled out approximately one millimeter and stuck back in, after which again ten series of twenty data points were taken. This procedure has been repeated once, so that a mean with its average deviation of these three measurements can be estimated. This uncertainty is calculated separately for each fiber and for gel and no-gel, so that it can be added to the uncertainty of the detector position of each measurement of the comparison:

		uncertainty through rotation
old fiber	no gel	±2.5%
	gel	±2.3%
new fiber	no gel	±1.2%
	gel	±0.6%

To examine the rotation in more detail, the minimum for each fiber-gel/no-gel combination was set in afterwards, as well as a rotation of 45° from the maximum:

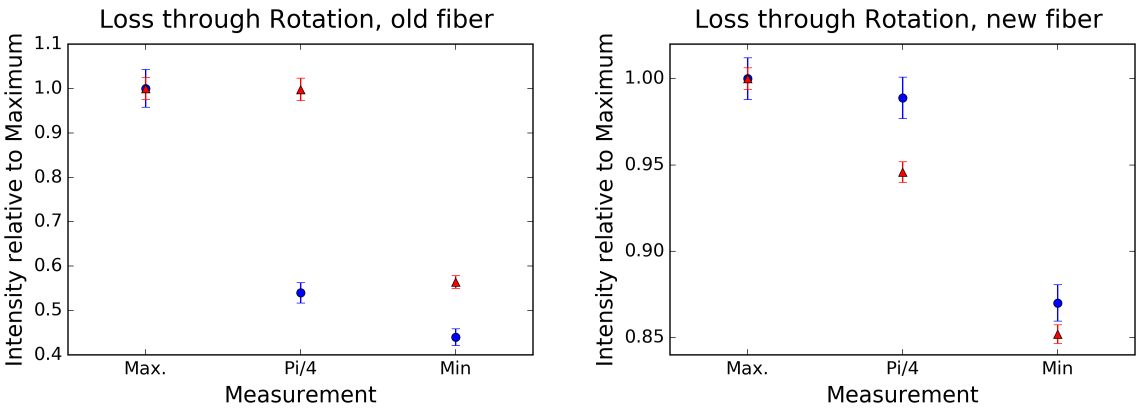

Figure 3.12: Deviation of intensity loss by fiber rotation. The error range has been estimated by searching the maximum three times. The red dots are from the coupling with gel, whereas the blue dots are from the coupling without gel.

In this test it seems, that the level of worn-out has a significant influence to the maximal deviation of the intensity at fiber rotation. While for the old fiber a maximal loss of 56% is detected, for the newer fiber a maximal loss of only 15% could be measured. The reasons that would explain a difference due to rotation are:

- a curvature of the the fiber, that could rotate the fiber end away from the sensitive area of the detector.
- skew fiber endings, which could emit the light away from the sensitive area, if the fiber does not end symmetrical in the middle of the detector.
- obliquely mounted sensor chips inside the detectors. Because they were attached by hand, there is no guarantee that they are perfectly mounted.

- slightly skewed position of the whole detector. With this setup a perfect right angle between the fiber and the detector cannot be ensured.
- effects of torsion, for example, at the coupling, which is unsymmetrical through the erosion of the fibers.

In another test, where the optical fiber leads directly from the Ulbricht-sphere to the detector, light losses of the same dimension like in the tests with the more used fiber from above were observed. This would indicate that the deviation originates from one of the first four effects mentioned before. Or probably a mixture of all of them. Unfortunately this cannot be resolved easily in this experimental setup.
To examine this more closely a detector would be needed, which allows the fiber to be stable attached to it. Unfortunately the used detectors do not measure anything, if the fiber touches the sensitive area, nor do they allow to see exactly how far the distance and position of the fiber is, relative to the sensor.

3.6 Conclusion

To compare the gel coupling with the non-gel coupling with its total uncertainties, the errors of the detector position and the ones emerging from the fiber rotation are summed up linearly.

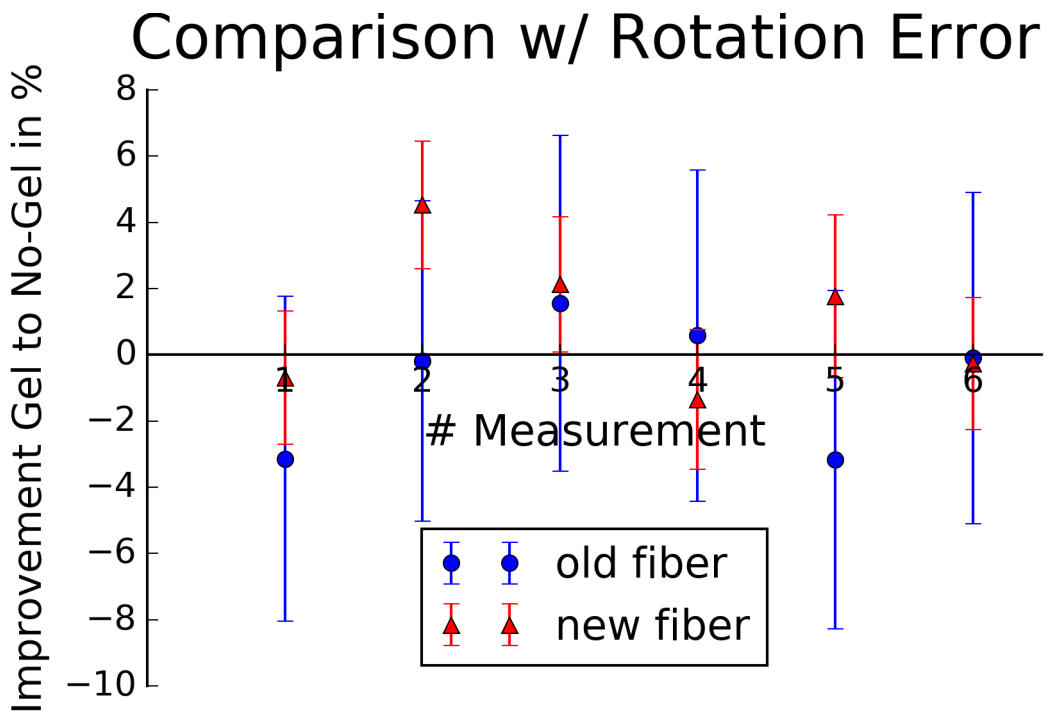

Figure 3.13: Final comparison of gel coupling to no-gel coupling. The error bars consist of the sum of uncertainties through detector position and rotation. The blue dots show the improvement from gel relative to no-gel with the older transparent optical fiber. The red dots show the data with of the newer fiber. The order is random and old and new fiber were measured independently. In average an improvement of $\approx 0.2\%$ can be determined. Consequently with the large error ranges a significant improvement could not be determined.

maximal improvement (in %)	4.52 ± 0.09 $(position) \pm 1.83$ $(rotation)$
maximal decline (in %)	-3.16 ± 0.58 $(position) \pm 4.52$ $(rotation)$
mean improvement (in %)	0.20 ± 3.53
theoretical estimation (in %)	≈ 9.7

In figure 3.13 the enlargement of the uncertainties through rotation are clearly recognizable. Because the values lay within their error ranges, the big deviation of the improvements can be traced back now to the uncertainty through slight fiber rotations, which cannot be easily be eliminated in this experimental setup. Altogether a slight improvement of $\approx 1.1\%$ can be detected with the new fiber, while a slight decline of $\approx 0.7\%$ (in average) is detected with the older fiber. Like described above, this difference might arise from different curvatures of the fibers, which could not be determined exactly.

The theoretical estimation of an improvement due to a coupling with gel cannot be confirmed yet.

With that comparison it gets clear, that this experimental setup is too imprecise to measure, whether gel improves the coupling or not.
Further investigation on fiber coupling is necessary. A possible setup to reduce the uncertainties would contain a sliding table, on which the fiber is fixed to the detector. Both elements could securely be moved together to put gel on the fiber ends.
Another possibility would be a second Ulbricht-sphere at the end of the optical fiber. Theoretically then the influence of the fiber curvature should not matter. However, the intensity, entering the detector, would decrease further, but could solve this issue by using a high efficiency SiPM.

The detailed values of this measurement are shown in the appendix in table 6.1.

CHAPTER 4

Reflective end

The second part, which is investigated in this thesis in regard to possible light losses, is the reflection at one end of the glued-in WLS fiber inside the tile of AMD.
For the measurements, which were compared to the simulation, the fiber end was painted with a chrome paint. It is to find out if and how much light is reflected back into the fiber. Also other materials have been studied to investigate if there are more practicable and better ways to prepare the fiber to reflect the light.

In this chapter at first a theoretical description of the light reflection at fiber ends follows. Then the basic idea of the experiment and of its setup is given. After that, the procedure of measuring is explained and finally a comparison of different materials as reflectors is shown. In the end consequences for AMD will be concluded.

4.1 Theory

One half of the light, that is trapped inside the WLS fiber, propagates in each direction of the fiber. If the fiber end, that is glued in the scintillator tile, is prepared with a reflector, the light, that travels to this end, would be reflected back into the fiber and is not lost. Hence ,the task is to get the light, that exits the fiber, back into it at an angle smaller than the acceptance angle of the fiber. Therefore some material could be attached to the fiber end. Different materials have different properties regarding to incoming light. There are two kinds of reflections: Diffuse reflection and specular reflection. While diffusely reflective materials macroscopically just appear bright, specularly reflective materials are mirroring the incoming light.
Ideal diffuse reflections describes the reflection of light rays uniform with equal luminance in all directions. For mirroring the incoming light, specularly reflecting materials satisfy that the angle of incidence equals the angle of reflection.
That means that if a specularly reflective material is attached directly to the fiber end, all the light that would exit the fiber at an angle smaller than the acceptance angle would be

reflected back into the fiber and would be transmitted because of total internal reflection. The challenge with diffuse reflection is the evenly distributed light. Only the part which is reflected at a smaller angle than the acceptance angle gets back into the fiber. All the other light is lost. One can calculate the difference between an ideal specular reflector and an ideal diffuse reflector:
The reflected light is distributed over half a spherical shell with a surface = 2π. Only light with an angle smaller than 35.7° is trapped in the fiber, this is a surface of

$$\int_0^{37.5^\circ} \int_0^{2\pi} sin(\theta) d\theta d\phi = 2\pi \cdot 0.2 \quad . \tag{4.1}$$

That means an ideal diffuse reflector only reflects 20% of the light, that a specular reflector reflects, back into the fiber.

4.2 Experimental setup

In the following experiment again relative measurements in comparison to each other have been performed.
In order to compare different reflective materials at the fiber end to each other and the fiber end without any material attached, the following experiment was built:

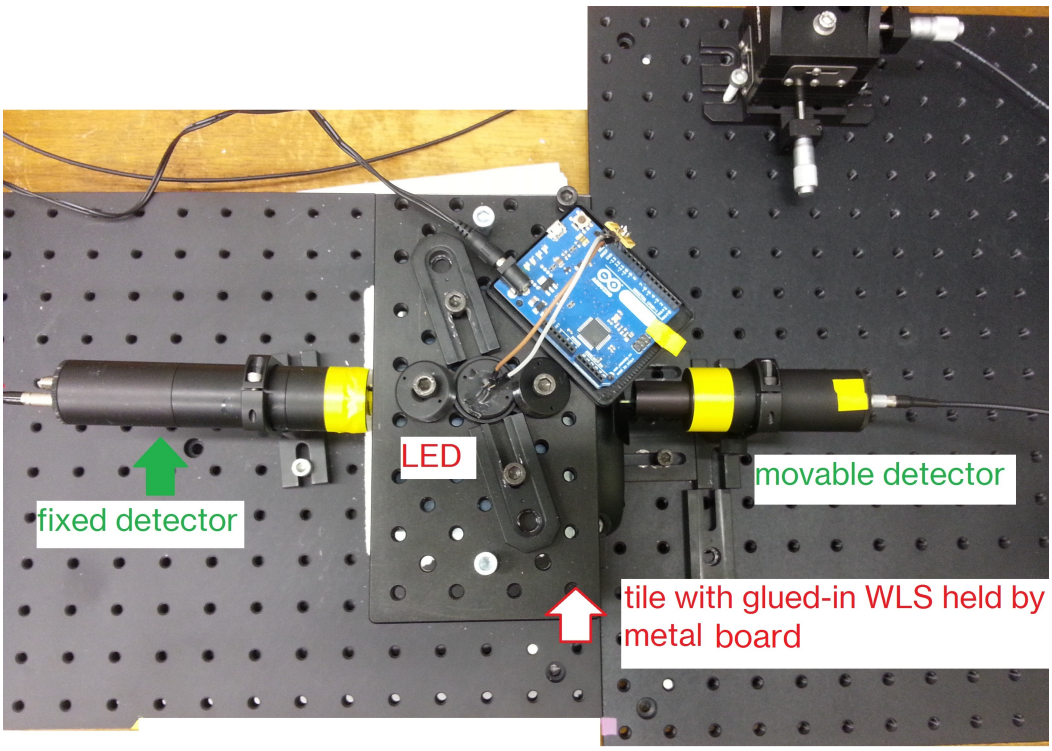

Figure 4.1: Experimental setup. The test tile is attached under the metal board. Light is induced via a LED on the top of this board.

The setup is built on a Thorlabs basement and the two detectors with the same read-out electronics as in chapter 3.
The perspex tile with the glued-in WLS fiber is clamped on a holding. To the short end of the WLS a detector is firmly attached. On the other end a movable detector with a similar guideway as in the previous chapter is set up. Due to the latter the amount of light that leaves the end of the fiber and gets through the chrome can be compared.
In a hole in the tile holding a LED is attached, so that the light is constantly induced to the WLS fiber from the side. For the first measurements this is the exact same (UV+blue)-LED, which was used in chapter 3 as well.
This way one fiber end is easily accessible for changes of the reflective materials.

4.3 Measurements

The basic idea of this experiment is to compare the increase of intensity at one fiber end while different materials are attached to the other side of the WLS fiber. By this way the material that reflects best is searched, as well as the reflection efficiency of the chrome paint, which is already used in the first scintillator tiles, is determined.

The experiment consists of three parts. For each part a different test tile with glued-in WLS fiber is used. Several tiles were necessary, as some methods of attaching material are permanent. Hence, to take more than one measurement with chrome a second tile with glued-in WLS fiber was needed. During the measurements with the first two tiles, it has been discovered, that the fiber ends that were meant to be made reflective, were not polished. -(Not the side with that was coupled during the first part of this thesis, those were polished)- Whereas the second tile had a more clean end than the first tile. For the reflection the polishing of the fiber end is crucial. At unpolished ends the light gets emitted at undefined angles, and the reflection back into the fiber becomes more unlikely. The fibers used in AMD are of course polished. To get significant data on reflection for this purpose, tests with a polished fiber end are needed. The physics workshop was able to remove the chrome paint with isopropyl alcohol and has polished the second tile, so it could be used again (this time with two polished ends), here called the third tile.

In this section the different experiments taken with each tile are explained.
For each test series ten measurements were taken. For the comparison the average of those ten measurements were calculated and its uncertainty was estimated with its variance.

The results of these measurements are shown in section 4.4.1.

4.3.1 First tile

The WLS fiber end of the first tile is the worst polished one.

With this tile, chrome as a reflector was investigated. A chrome spray, from 'Motip Dupli', bought in a building supplies store, was used. After DIN 67530, it is shiny at an angle of 60°. This spray was also used, to make the fiber ends in the first scintillator tiles reflective. To paint the fiber end, it was sprayed onto a piece of paper, so that a little puddle of paint was created. Before the chrome dried, it has been painted on the fiber, so that no area of the fiber end remained uncovered.
To examine the use of different amounts of chrome, six measurements were taken. One without chrome at all, as base for the comparison, and five with different layers and different amounts of lateral fiber area being painted (see figures 4.2-4.7). For the first layers the chrome did not consistently cover the fiber end (figure 4.3). In the following table the properties of each chrome layer are described, as well as the improvement through reflection. For these tests the movable detector was positioned at the painted fiber end, so the amount of light that has passed through the chrome, hence a degree of how opaque each layer is, is shown too. All measurements are relative to the open fiber end.

#	layers	Millimeter painted	increase due to reflection	decline of passed light
1	1	5	3.1%	97.1%
2	2	5	2.2%	99.3%
3	2	10	2.1%	99.3%
4	3	10	2.1%	99.8%
5	4	15	2.1%	99.8%

With only one layer of chrome, the highest increase, so the highest reflection efficiency, has been measured. On the other hand, this measurement showed the largest amount of light leaving the fiber end. This and the fact that all measurements show almost no increase of intensity at all, might indicate that the chrome paint absorbs the light, or reflects it to higher angles. This will be discussed in more detail later.

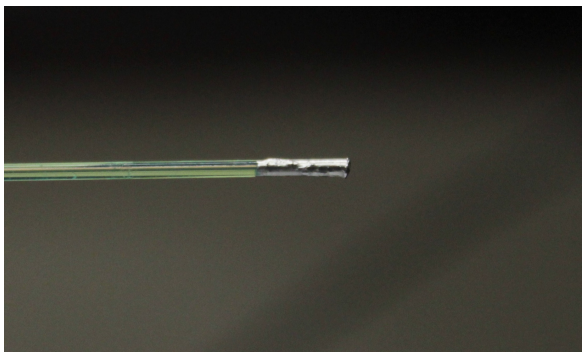

Figure 4.2: One layer of chrome, 5 mm painted.

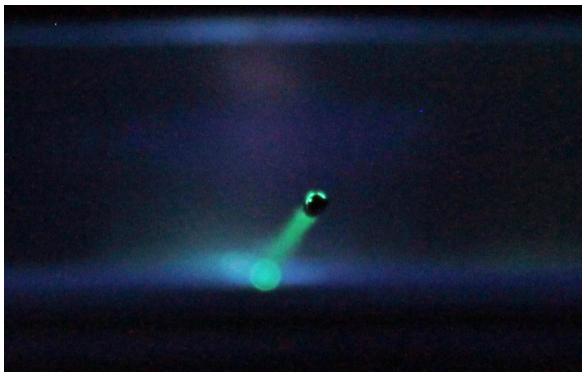

Figure 4.3: The first layer does not cover the fiber end completely. Clearly visible: light comes through the chrome.

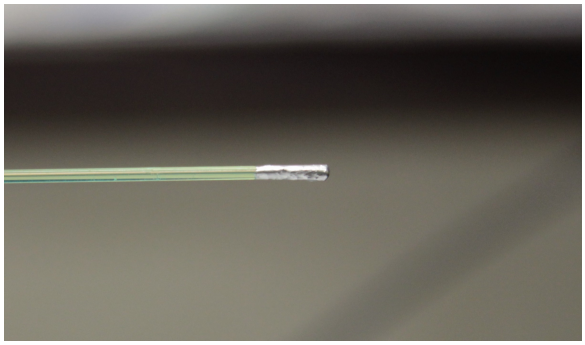

Figure 4.4: Two layers of chrome, 5 mm painted.

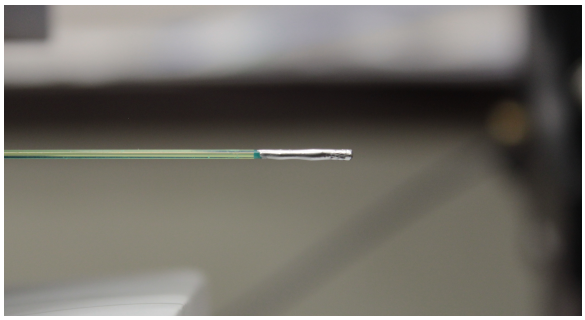

Figure 4.5: Two layers of chrome, 10 mm painted.

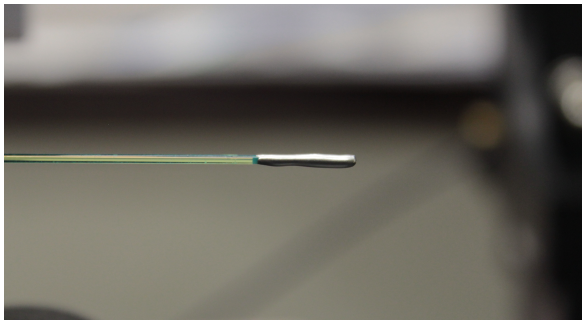

Figure 4.6: Three layers of chrome, 10 mm painted.

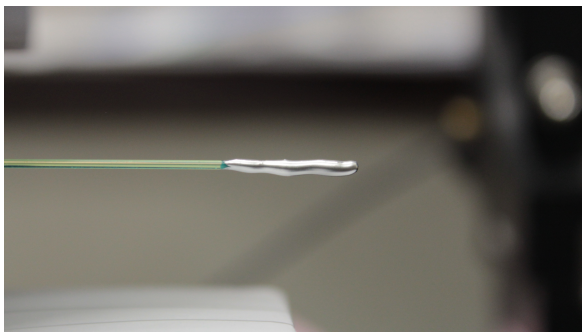

Figure 4.7: Four layers of chrome, 15 mm painted.

4.3.2 Second tile

The fiber end of this tile is more polished than the one from the first tile, but irregularities could still be seen with bare eyes.

With this tile five tests were made. At first a little cylinder was built with a special reflecting foil like seen in figure 4.8 and 4.9. The detailed properties of this foil are not known, only that its reflectivity is higher than 80%. If with such a cylinder a larger increase of intensity is measured as with chrome, a possible way to attach a reflective material at the fiber ends would be found. Due to the asymmetry of the cylinder, several measurements with different cylinder positions (rotation) were made. For the later comparison the data from the position with the greatest improvement are taken. To compare the increase in intensity due to the reflection, an additional measurement without the cylinder was taken.
Afterwards two cylinders of different kinds of tyvek were built (figures 4.10-4.11). Tyvek©[18] is a mainly diffusely reflective material. These cylinders were more symmetrical, so that a rotation did not change the reflection. For each of those a additional measurement with the open fiber end was made.

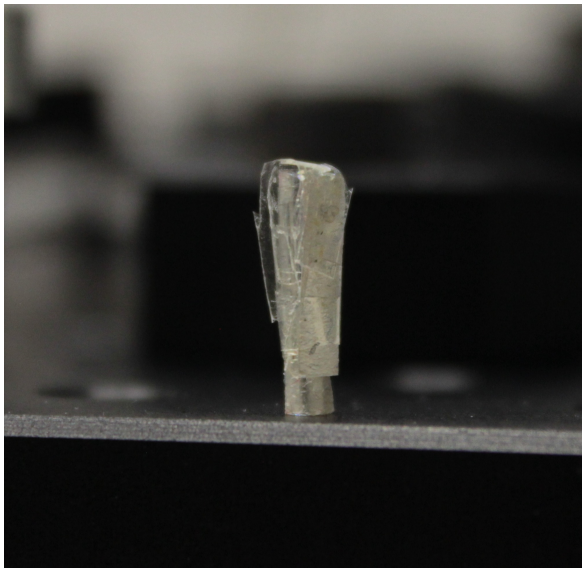

Figure 4.8: Cylinder made of reflective foil.

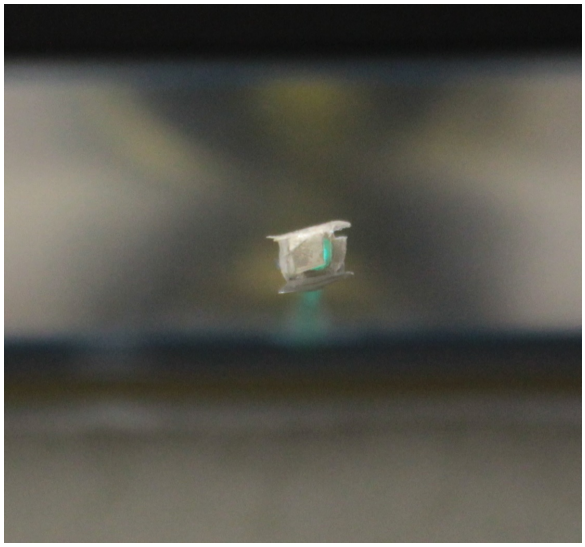

Figure 4.9: Due to its width of some millimeters, the cylinder could not be built perfectly.

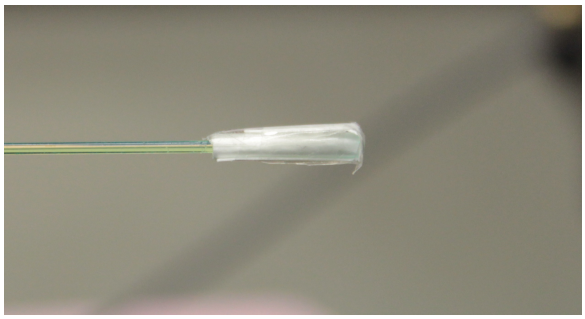

Figure 4.10: Cylinder built of Tyvek material.

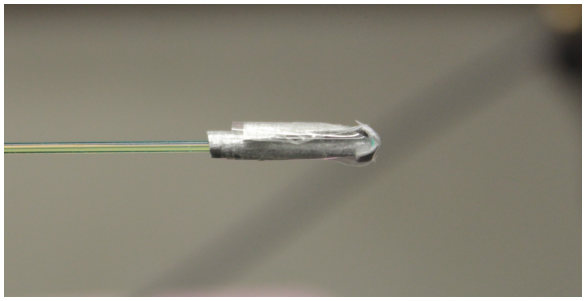

Figure 4.11: Cylinder built of another Tyvek material.

Then tests with plane pieces of reflective foil were made, onto which the fiber is positioned. For that purpose foil has been stuck on a Thorlabs element, which was easy to move on the platform and solid enough to not dangle while measurements. To position this element a guideway similar to the one from chapter 3 was attached. It is shown in figure 4.12. To estimate the uncertainty through possible small variations in position or angle, the element is repositioned ten times for each measurement. From its deviation the uncertainty is estimated through its variance.

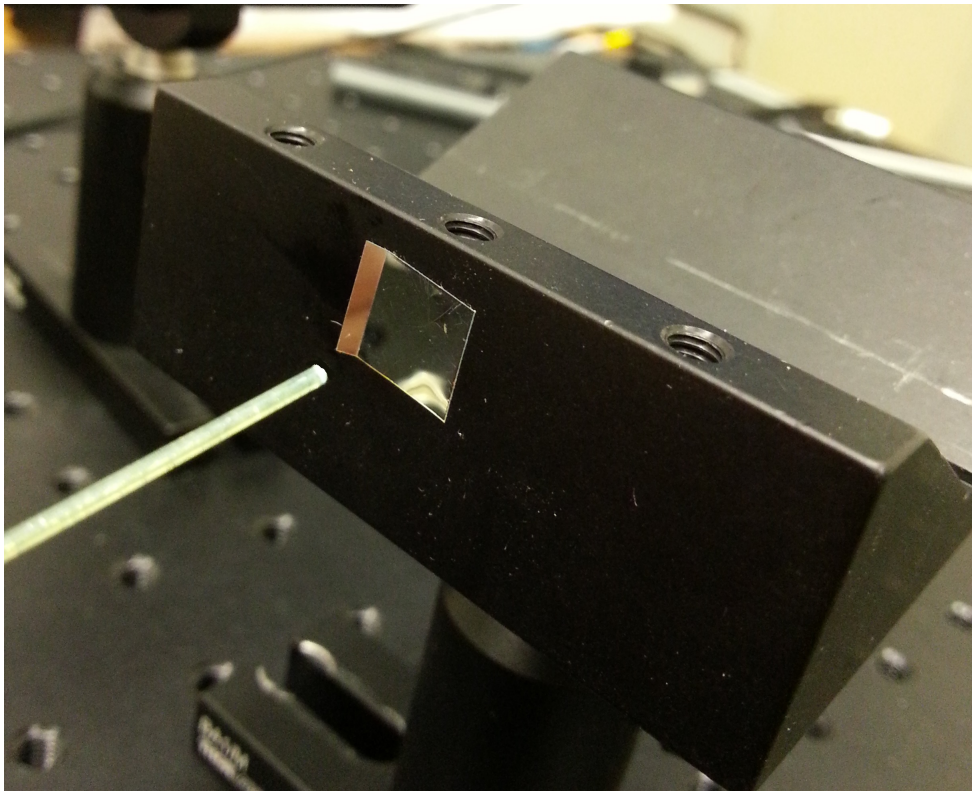

Figure 4.12: Thorlabs element attached with reflective foil for reflection tests at a plane surface.

The last test with this tile was again a series of measurements with chrome. For this purpose the same procedure as described in section 4.3, has been used.

4.3.3 Third tile

For the largest test series, the fiber end of one tile was repolished.

At first, tests with planely mounted materials were made. This time with the two different tyvek materials; with PTFE [19], which also is a mainly diffuse reflector; with the reflective foil already used before; and with another reflective foil, whose properties, besides its reflectivity better than 80%, unfortunately are not known either. In addition the test with the first reflective foil has been repeated with gel between fiber end and foil. Each measurement is performed with the same procedure as before. So each measurement contains ten repetitions.

Also the measurements with the three cylinders were repeated.

To quantify the intrinsic reflection of the uncovered fiber end due to the transition WLS to air, an additional test was made. For this purpose the fiber was held in water. Water has a refractive index of about 1.3 so that theoretically about 0.8% of the light should be reflected at the end (instead of about 5.5% in air). To place the fiber end in water, but still being able to measure the reflection, a cup of water with a tiny hole has

been positioned at the fiber end. This measurement was repeated one time, but with no difference of reflected intensity. For comparison a measurement with the open fiber end was taken.

The final test is to find out a possible way to effectively make the fiber end inside the scintillator tiles reflective. For this purpose a small piece of reflective foil (here, the second foil has been used) was cut out and glued onto the fiber end. The same optical cement (BC 600 from 'Saint-Gobain' [20]) that is used to glue the fiber in the scintillator tile, has been applied. Before the foil was permanently glued on the fiber end, again a measurement with the uncovered fiber end was taken.

4.4 Comparison of different materials as reflectors

4.4.1 Comparison

To compare the improvement due to reflection of the different materials, the difference between each reflection measurement and its control measurement has been calculated. Then, to get the absolute increase due to reflection, all these differences are shown relative to the measurement of water. The measurement with water should give a value of how much intensity reaches the detector with a non-reflective end located in the tile. In comparison to the open fiber end without water, the intensity declines about 3.7%. This decline approximately matches the theoretical estimation of about 5%.

Due to the statistical identity of the uncertainties of the averages of the taken measurements, they can be summed up quadratically to estimate the uncertainty of the difference.

In figure 4.13 only one average of ten measurements for each chrome test is taken. The difference of the several chrome layers was less than one percent, so only the measurement with highest increase is shown. For the tests with the reflective foil cylinders, where several measurements per test have been taken due to its asymmetry of rotation, only the measurement with the highest increase has been taken.
Absolute values of these measurements are shown in the appendix in tables 6.2-6.4. The biggest improvement due to reflection is $(70.7 \pm 3.9)\%$. This was detected with reflective foil coupled onto to fiber with optical gel. That was expectable, because reflective foil is a specular reflector.
Another interesting observation is, that the increase through reflective foil with the unpolished tiles are approximately as good as the increase through the diffuse reflectors with the polished tile. That makes sense, as the light at the unpolished fiber end probably is emitted more diffusely than the one from the polished fiber end.
The fact that the increase through diffuse reflectors is more than the theoretically calculated 20% of the direct reflected light, can be explained with the non ideal diffuse reflection of the materials.

One can see, that the glued piece of reflective foil does not increase the intensity as good as the plane reflective foil, which is attached with gel. A possible explanation could

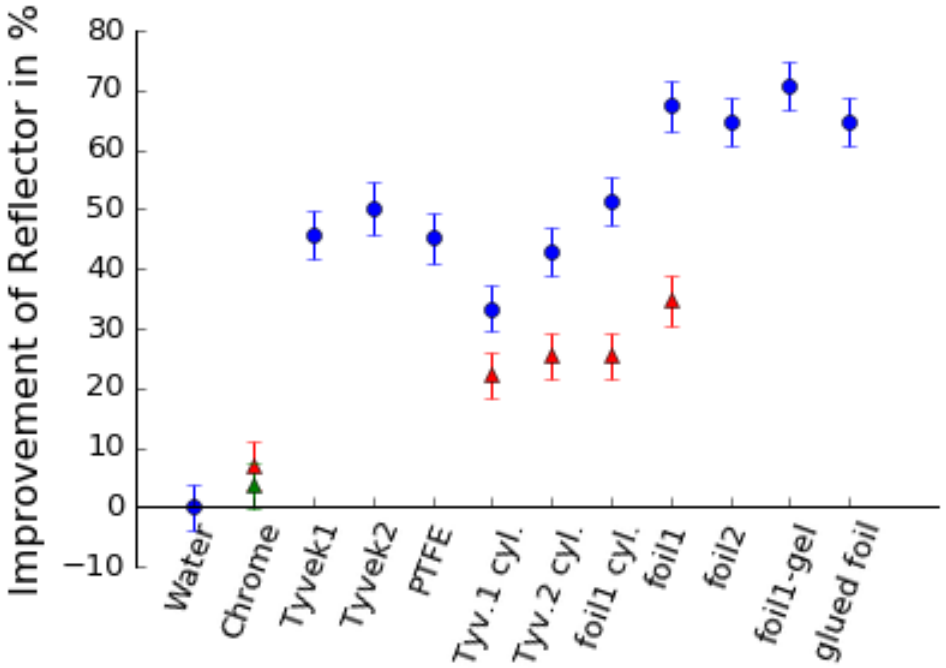

Figure 4.13: The different improvements of intensity due to different reflective materials are shown. The green and red triangles show the measurements of the first, respectively the second tile, while the blue dots show the measurements with the third (polished) tile. All increases are shown relative to the decline, which was measured due to absorption by water on the one end of the fiber.

be, that the glued foil piece had to be hold in place for 24 hours to dry. This was realized by carefully pushing a solid object against the fiber end with the piece of foil in between. It may be that the foil is glued onto the fiber a little inclined. With bare eyes this could not be ruled out.
Nevertheless the difference to the maximal measured increase is not very big and the improvement compared to chrome is very good.

4.4.2 Chrome

At first thought, the chrome paint should work as a reflector. As verified by spraying it onto a flat, clean surface.
To find out, why it is not reflective on the fiber ends, a fiber was stuck into the paint very carefully, so that only the footprint of the fiber is painted. After it dried, it was examined under a microscope. For that purpose only a short piece ($\approx 3\,\text{cm}$) of transparent optical fiber was used. This is so short, that one was able to see through it from the other side of the fiber.
By doing so, one could recognize that the chrome does not dry as one plane surface, but as a mixture of shiny spots, dark crater-like structures and cracks. So a probable explanation for the light loss could be a mixture of reflections, so that parts of the fiber reflect diffusely, while others, like the cracks, mainly absorb the light, and other parts,

like the shiny spots, reflect well, but probably at an angle higher than the acceptance angle of the fiber.

4.4.3 Additional losses

One could think that the optimum of reflection should be 100%, but the maximal measured increase is about 70%. There are different factors that may explain the missing increase:

- non-perfect reflection: It is not clear, if the used reflective foil is the absolute best reflector. Especially because the properties of the foil are not exactly known. Several percent are probably lost through this. By testing a foil with a known reflectivity of $98 - 99\%$ one could solve this problem.
- attenuation length: there is a light loss depending on the distance that the light has to propagate inside the fiber. The light, that gets reflected has to travel a longer way; about 26 cm more. In the WLS fiber about 63% of the light is lost after 3.5 m. Hence, about 5% of the reflected light is lost compared to the direct light.
  This is the main issue of the WLS in the scintillator tiles. The loss due to the attenuation length cannot be reduced.
- imperfections of the experimental setup. It may be that some light is reflected at the holding of the tile or similar and gets into the detector, even though there is only a small hole besides the fiber in which light could enter the detector.
- losses through the interface of the lateral fiber area with air may cause some percent loss of intensity [12].
  This effect is reduced in the scintillator tiles, due to the similar refractive index of the optical cement, with which the fiber is glued-in.
- wavelength depending effects like a non perfect absorption inside the WLS fiber, which leads to a small amount light entering the detector through the fiber directly, while the same amount of light propagating in the other direction cannot make all the way to the other fiber end and the way from the reflection into the detector, due to the bigger distance, if it is not trapped inside the WLS fiber.

The last of the five effects should not make a significant difference, because the used (UV+blue)-LED emits light with a spectrum very near the maximum of the absorption spectrum of the WLS fiber.

In addition, these effects could explain the missing percent.

4.5 Conclusion

In this chapter it was shown, that the chrome paint, with which the WLS fiber ends in the first tiles were painted, is not very efficient for this purpose.
A significant improvement was seen with reflective foil. With it, increases of intensity at the opposite fiber end of about 70% have been measured. It was estimated that this approximates the possible maximum of intensity increase with the experimental setup and materials used.
A practicable way to make the fiber ends, that get glued in the scintillator tiles for AMD, reflective, could be a small piece of reflective foil that is glued onto the polished fiber.
Attention has to be paid on how the piece of foil is glued onto it. Any non parallel orientation of the foil would probably lead to a loss of intensity.

CHAPTER 5

Conclusion and outlook

To find explanations for the difference in light yield between simulations and measurements with prototype scintillator tiles of the Aachen Muon Detector, two different parts of the light conducting system were investigated on. The coupling of the WLS fiber to the transparent optical fiber and the reflection at the fiber end, that is glued inside the scintillator tile.
The measurement, which is compared to the simulations, was made with a coupling, where both of the fibers were just stuck together in the clamp. In the first part of this thesis it was shown by calculations, that a possible light loss of about 9% could be avoided by coupling the fibers with optical gel. However, the performed experiment could not find a significant difference between the coupling with gel and the coupling without gel. It is possible, that sticking the both fiber ends together already is a almost perfect coupling, even if it seems not that probable, but it turned out, that the experimental setup was too imprecise to measure a certain improvement of several percent.
In the other part of this thesis it could be shown, that the so far used chrome paint does not work effectively as a reflector at the fiber end. Another suitable method and material to reflect a significant amount of about 70% of light was developed and tested. For this method a piece of specularly reflective foil is glued onto the fiber end.

Due to the much longer distance the light has to travel in the scintillator tile, the loss through the attenuation length of the WLS fiber prevents the actual improvement of $70 - 80\%$, with highly reflective foil glued to the fiber end. Hence, only an roughly estimated improvement of $\approx 50\%$ would be possible due to reflection.

Even though there is still a significant difference between the simulation and measurement, a part of this difference could be explained and can probably be reduced in the future.

CHAPTER 6

Appendix

Measurement vs. simulation

In the following section a comparison between the light yield of the prototype of the light conducting system and the scintillator tiles of AMD, with an estimation via simulation, is explained.
To measure the light yield, a test shelf (seen in figure 6.1) was built by the mechanical workshop of the III. Phys. Inst. of RWTH Aachen University. This shelf allows different test set-ups of the components (see chapter 2) and provides easy access to them. For this measurement eight tiles were set up in the shelf. Four of these tiles (the very first and last , as well as two other tiles in between, where used as a coincidence triggers for muons traveling through the shelf. Due to this set-up an almost pure muon, so a highly noise reduced, sample is achieved.
For the measurement the electronics signal of the SiPMs has been translated into amounts of detected photon equivalents (p.e.). A threshold of 2.5 p.e. is used. In figure 6.2 the MIP (minimal ionizing particle) muon signal, starting at the 1 p.e. peak, of one tile, which is triggered by the fourfold coincidence, is shown.

On the other hand, the distribution of detected photons at the SiPM for many single muons in the MIP energy range, uniformly distributed over an AMD tile of the very first design, is simulated. For this purpose a threshold of 10.5 p.e. is used to significantly reduce noise effects.
The simulation is based on a dedicated Geant4 simulation framework, which includes the complete detection system of AMD as well as the electronics read-out.

One has to mention, that measurement and simulation do not represent the exact same experimental set-up and measurement chain. However, the large discrepancy between the both becomes clearly visible. Even though the simulated amount of detected photons can be adjusted by modifying parameters of the simulation, detailed and appropriated measurements are needed to identify reasonable causes of light losses in the

set-up in comparison to the simulation.
Due to the differences of the experimental setup to the design simulation, the factor of how much worse the photon yield of the measurement is, can only be roughly estimated to approximately 4 to 5 (see figure 6.2).

The simulation was made by Tim Niggemann and Christine Peters.
The measurement was performed by Rebecca Meissner and Lukas Middendorf.

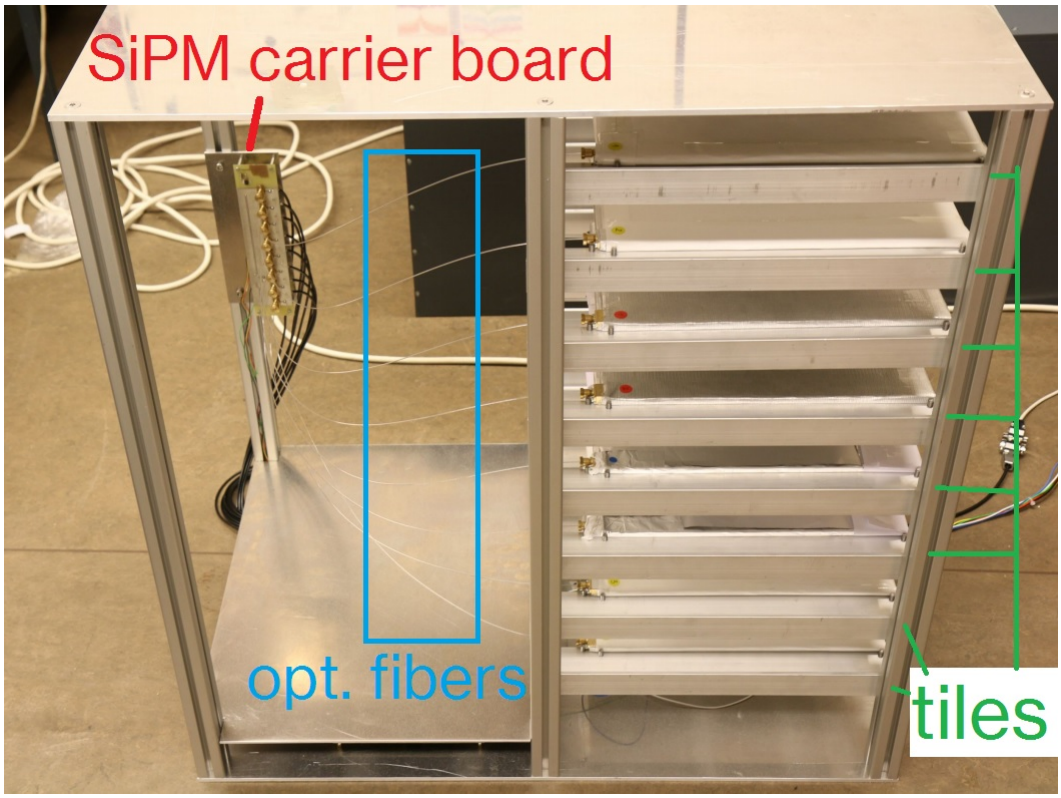

Figure 6.1: Test shelf, in which eight scintillator tiles are placed.

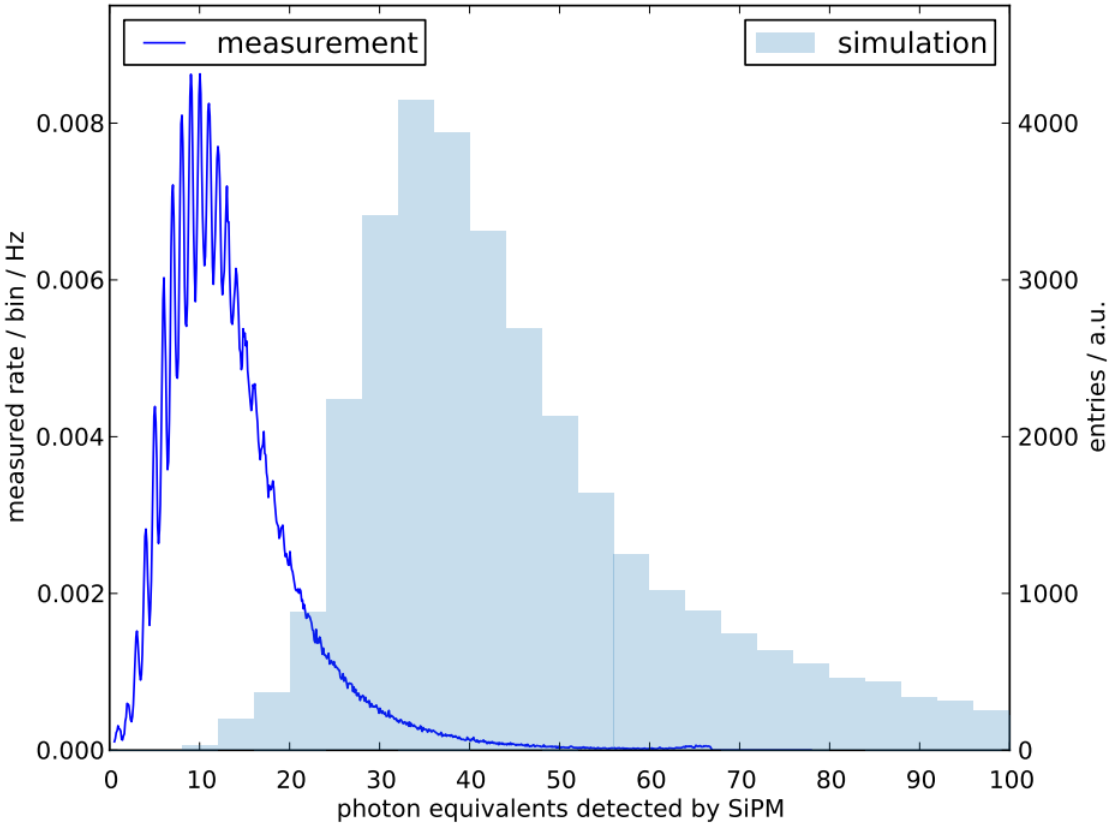

Figure 6.2: Comparison between the simulation and the measurement of light yield with the components of AMD. Even though they do not represent the exact same experimental set-up and measurement chain, the large difference indicates light losses in the measurement.

Fiber coupling

#	$\frac{(\text{gel} \pm detector position \pm rotation)\cdot 10^{-9}}{(\text{no-gel} \pm detector position \pm rotation)\cdot 10^{-9}}$	$(\Delta \pm det.pos. \pm rot.)\cdot 10^{-9}$	% to no-gel
1	$2.036 \pm 0.007 \pm 0.023$ $2.102 \pm 0.0035 \pm 0.025$	$-0.066 \pm 0.008 \pm 0.099$	$-3.139 \pm 0.372 \pm 4.727$
2	$2.130 \pm 0.004 \pm 0.023$ $2.134 \pm 0.003 \pm 0.025$	$-0.004 \pm 0.005 \pm 0.102$	$-0.187 \pm 0.234 \pm 4.795$
3	$2.080 \pm 0.008 \pm 0.023$ $2.048 \pm 0.004 \pm 0.025$	$0.032 \pm 0.009 \pm 0.099$	$1.562 \pm 0.436 \pm 4.836$
4	$2.077 \pm 0.003 \pm 0.023$ $2.065 \pm 0.007 \pm 0.025$	$0.012 \pm 0.008 \pm 0.099$	$0.581 \pm 0.386 \pm 4.813$
5	$1.989 \pm 0.011 \pm 0.023$ $2.054 \pm 0.005 \pm 0.025$	$-0.065 \pm 0.012 \pm 0.097$	$-3.164 \pm 0.588 \pm 4.727$
6	$2.015 \pm 0.006 \pm 0.023$ $2.017 \pm 0.005 \pm 0.025$	$-0.002 \pm 0.008 \pm 0.096$	$-0.099 \pm 0.411 \pm 4.797$
1	$2.610 \pm 0.004 \pm 0.006$ $2.628 \pm 0.004 \pm 0.012$	$-0.018 \pm 0.005 \pm 0.047$	$-0.685 \pm 0.215 \pm 1.796$
2	$2.725 \pm 0.002 \pm 0.006$ $2.607 \pm 0.0015 \pm 0.012$	$0.118 \pm 0.002 \pm 0.047$	$4.526 \pm 0.096 \pm 1.827$
3	$2.637 \pm 0.003 \pm 0.006$ $2.582 \pm 0.005 \pm 0.012$	$0.055 \pm 0.006 \pm 0.046$	$2.130 \pm 0.226 \pm 1.813$
4	$2.487 \pm 0.002 \pm 0.006$ $2.521 \pm 0.008 \pm 0.012$	$-0.034 \pm 0.008 \pm 0.045$	$-1.348 \pm 0.326 \pm 1.792$
5	$2.546 \pm 0.0025 \pm 0.006$ $2.502 \pm 0.016 \pm 0.012$	$0.044 \pm 0.016 \pm 0.045$	$1.758 \pm 0.647 \pm 1.810$
6	$2.577 \pm 0.003 \pm 0.006$ $2.584 \pm 0.004 \pm 0.012$	$-0.007 \pm 0.005 \pm 0.046$	$-0.271 \pm 0.193 \pm 1.798$

Table 6.1: Detailed values of the comparison measurements of gel and no-gel used for coupling. The first six rows contain the measurements with the older fiber, while the latter show the values of the newer fiber. The values are in units of Ampere.

Reflective end

#	$\frac{\text{with reflector } \cdot 10^{-9}}{\text{without } \cdot 10^{-9}}$	Difference $\cdot 10^{-9}$	improvement in % to water
Chrome	6.398 ± 0.0006 6.410 ± 0.0007	-0.012 ± 0.001	3.68 ± 3.89

Table 6.2: Reflective end: measurements with first tile. The values are in units of Ampere.

#	$\frac{\text{with reflector } \cdot 10^{-9}}{\text{without } \cdot 10^{-9}}$	Difference $\cdot 10^{-9}$	improvement in % to water
Chrome	5.9224 ± 0.0003 5.7451 ± 0.0006	0.1773 ± 0.0007	7.08 ± 3.88
Tyvek1 cyl.	6.7370 ± 0.0005 5.7263 ± 0.0005	1.010 ± 0.0007	22.20 ± 3.90
Tyvek2 cyl.	6.9252 ± 0.0004 5.7346 ± 0.0003	1.1906 ± 0.0005	25.44 ± 3.88
foil1 cyl.	6.8622 ± 0.0006 5.6835 ± 0.0009	1.1786 ± 0.0011	25.41 ± 3.89
foil1	7.5586 ± 0.0120 5.8309 ± 0.0005	1.7276 ± 0.0120	34.65 ± 4.08

Table 6.3: Reflective end: measurements with second tile. The values are in units of Ampere.

#	$\frac{\text{with reflector } \cdot 10^{-9}}{\text{without } \cdot 10^{-9}}$	Difference $\cdot 10^{-9}$	improvement in % to water
water	5.1435 ± 0.0012 5.3430 ± 0.0004	-0.1993 ± 0.0013	0
Tyvek1	7.4342 ± 0.0150 5.2983 ± 0.0030	2.1359 ± 0.0091	45.75 ± 4.05
Tyvek2	7.7008 ± 0.0090 5.3231 ± 0.0004	2.3777 ± 0.0301	50.27 ± 4.46
PTFE	7.4238 ± 0.0213 5.3131 ± 0.0005	2.1107 ± 0.0198	45.14 ± 4.26
Tyvek1 cyl.	6.8319 ± 0.0003 5.323 ± 0.0003	1.5089 ± 0.0003	33.32 ± 3.88
Tyvek2 cyl.	7.3327 ± 0.0002 5.328 ± 0.0005	2.0045 ± 0.0005	42.95 ± 3.88
foil1 cyl.	7.7645 ± 0.0126 5.3243 ± 0.0005	2.4397 ± 0.0120	51.47 ± 4.11
foil1	8.5362 ± 0.0113 5.2991 ± 0.0003	3.2371 ± 0.0100	67.33 ± 4.07
foil2	8.4977 ± 0.0124 5.3647 ± 0.0002	3.1329 ± 0.0100	64.53 ± 4.06
foil1 gel	8.6942 ± 0.0041 5.2896 ± 0.0019	3.4046 ± 0.0044	70.73 ± 3.96
glued foil	8.4492 ± 0.0068 5.3248 ± 0.0013	3.1244 ± 0.0071	64.82 ± 4.01

Table 6.4: Reflective end: measurements with third tile. The values are in units of Ampere.

Bibliography

[1] Viktor Hess. Über beobachtungen der durchdringenden strahlung bei sieben freiballonfahrten. *Phys.Zeitschrift XIII*, 1912. URL https://www.mpi-hd.mpg.de/hfm/HESS/public/HessArticle.pdf.

[2] Antoine Letessier-Selvon and Todor Stanev. Ultrahigh energy cosmic rays. *Rev. Mod. Phys.*, 83:907–942, Sep 2011. doi: 10.1103/RevModPhys.83.907. URL http://arxiv.org/pdf/1103.0031v1.pdf.

[3] Karl-Heinz Kampert and AlanA. Watson. Extensive air showers and ultra high-energy cosmic rays: a historical review. *The European Physical Journal H*, 37 (3):359–412, 2012. ISSN 2102-6459. doi: 10.1140/epjh/e2012-30013-x. URL http://arxiv.org/pdf/1207.4827v1.pdf.

[4] K.A. Olive et al. (Particle Data Group. Review of particle physics. *Chin. Phys. C38*, pages 14–16, chapter 28, 2015. URL http://pdg.lbl.gov/2015/reviews/rpp2015-rev-cosmic-rays.pdf.

[5] Rebecca Meissner. Master thesis: Development and characterisation of a scintillator based muon detector with sipm readout for air shower experiments. *RWTH Aachen*, 2015.

[6] The Pierre Auger Collaboration. Muons in air showers at the pierre auger observatory: Mean number in highly inclined events. *Physical Review D*, pages 4–5, 2015. URL https://arxiv.org/pdf/1408.1421v6.pdf.

[7] The Pierre Auger Collaboration, A. Aab, P. Abreu, M. Aglietta, E. J. Ahn, I. A. Samarai, I. F. M. Albuquerque, I. Allekotte, P. Allison, A. Almela, and et al. The Pierre Auger Observatory Upgrade - Preliminary Design Report. *ArXiv e-prints*, April 2016. URL http://arxiv.org/pdf/1604.03637v1.pdf.

[8] The Pierre Auger Collaboration. The pierre auger cosmic ray observatory. *Nuclear Instruments and Methods in Physics Research Section A: Accelerators, Spectrometers, Detectors and Associated Equipment*, 798:1–11, 2015.

ISSN 0168-9002. doi: http://dx.doi.org/10.1016/j.nima.2015.06.058. URL http://arxiv.org/pdf/1502.01323v5.pdf.

[9] Peters, C. et al. The muon detector prototype AMD for the determination of the muon content in UHECRs. 2015. URL http://pos.sissa.it/archive/conferences/236/596/ICRC2015$_5$96.*pdf*.

[10] Eljen Technology. EJ-212 Plastic Scintillator. URL http://www.eljentechnology.com/images/products/data$_s$*heets*/$EJ-200_EJ-204_EJ-208_EJ-212.pdf$.

[11] Saint Gobain. WLS Fibers. . URL http://www.crystals.saint-gobain.com/uploadedFil 20Fibers 20Brochure.pdf.

[12] Simon Nieswand. Master thesis: Measurement of the exit characteristics of light from optical multimode plastic fibres. *RWTH Aachen*, 2014.

[13] Edmund Optics. Optical Grade Plastic Optical Fiber . URL http://www.edmundoptics.de/optics/fiber-optics/optical-grade-fiber-optics/02534/.

[14] Hamamatsu. S12571-050 SiPM . URL http://www.alldatasheet.com/datasheet-pdf/pdf/5

[15] W.Demtröder. *Experimentalphysik 2 - Elektrizität und Optik, page 239*. Springer, 2009.

[16] Saint Gobain. BC-630 Silicone Optical Grease . data sheet:. . URL http://www.crystals.saint-gobain.com/uploadedFiles/SG-Crystals/Documents/Organic 20Product 20Accessories 20Data 20Sheet.pdf.

[17] Texas Instruments. Temperature Sensore . URL http://www.ti.com/lit/ds/symlink/lm94021.pdf.

[18] DuPont. Hardstructure Tyvek 1082D . URL http://www2.dupont.com/Tyvek$_G$*raphics*/en_U

[19] PTFE Thread Seal Tape. 60g per m2 .

[20] Saint Gobain. Optical Cement . URL http://www.crystals.saint-gobain.com/uploaded 20BC600 20Data 20Sheet.pdf.